Journal of Hydrology: Regional Studies 50 (2023) 101581

Contents lists available at ScienceDirect

Journal of Hydrology: Regional Studies

journal homepage: www.elsevier.com/locate/ejrh

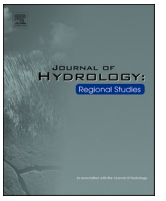

Drought characteristics projections based on CMIP6 climate change scenarios in Syria

Shifa Mathbout *, Javier Martin-Vide, Joan Albert Lopez Bustins

Climatology Group, University of Barcelona, Department of Geography, 08001 Barcelona, Spain

ARTICLE INFO

Keywords:
Syria
Mediterranean
Drought features
SSP
CMIP6
CRU TS
4.06
ERA5
SPI
SPEI

ABSTRACT

Study region: Syria
Study focus: This study delves into predicting drought characteristics in Syria, focusing on their duration, frequency, and intensity. It utilizes a set of 13 models sourced from the latest CMIP6 dataset, encompassing two distinct SSP scenarios. To evaluate how well CMIP6 represents drought attributes in Syria, the research conducts a comparison with observed monthly climate data from CRU TS v4.06 and ERA 5, as well as the CMIP6 model ensemble outputs for the reference period (1970–2000).
New hydrological insights for the region: This study provides new hydrological insights for Syria. It reveals robust projections of increasing drought severity, frequency, and duration, particularly in the north and northeast arid and semi-arid regions, even under aggressive climate mitigation scenarios. Additionally, the study highlights that higher emissions scenarios are associated with more prolonged and intense drought events, potentially impacting even less vulnerable areas. These findings emphasize the urgent need for drought adaptation and mitigation measures, as well as improved water resource planning, in order to address the changing hydrological landscape of the region. Furthermore, it underscores the long-lasting effects of drought on ecosystem recovery, which may span several decades.

1. Introduction

Global warming, driven by both natural and anthropogenic forces, has profound implications for the Earth's hydrologic cycle, leading to a reduction in terrestrial water availability (Padrón et al., 2020; Ballarin et al., 2021). It also alters the frequency and intensity of precipitation events (Martel et al., 2021; Zhao and Dai, 2022). The Mediterranean region (MED) stands out as a climate change hotspot (Lionello and Scarascia, 2018), experiencing a more rapid annual temperature increase than the global average (Cramer et al., 2018). Projections indicate that in the MED, droughts are expected to become both more severe and frequent as global warming exceeds 1.5 °C (Lionello and Scarascia, 2018; Tramblay et al., 2020). Adaptation to the changing climate is paramount for Mediterranean countries, particularly those in the eastern and southeastern Mediterranean, which face substantial vulnerability to climate variability and are ill-prepared for the socioeconomic shocks that accompany climate change (Abel et al., 2019). Future Mediterranean climate characteristics are closely tied to thermodynamic factors such as land-ocean warming contrasts and summer lapse rate changes (Brogli et al., 2019) and dynamic shifts like alterations in upper-tropospheric large-scale circulation patterns during winter (Tuel and Eltahir, 2020). Recent observations point to an accelerated transition to a more arid climate in several regions,

* Corresponding author.
E-mail address: shifamathbout@yahoo.com (S. Mathbout).

https://doi.org/10.1016/j.ejrh.2023.101581
Received 10 July 2023; Received in revised form 24 September 2023; Accepted 16 November 2023
Available online 18 November 2023

including the MED, driven by increased warming, prolonged droughts, and population growth (Ozturk et al., 2018; Cammarano et al., 2019; Barcikowska et al., 2020). This projected escalation of warming (Cos et al., 2022; Deng et al., 2022) and droughts across the MED in the coming century may exacerbate social tensions, leading to conflicts, human mobility, and migration (Adger et al., 2021). Understanding how dry spells will evolve in the future is critical for building resilience to these drought events (Breinl et al., 2020; Adeyeri et al., 2023). Syria, situated at the crossroads of Asia and the Mediterranean, is a highly water-stressed region prone to severe droughts, with temperature and evaporation playing significant roles (Barlow et al., 2016; Mathbout et al., 2018; Alsafadi et al., 2022). Most of Syria's drylands are trending toward increased aridity, especially in the northeast, and a substantial portion of the central arid region has already transitioned to a hyper-arid state (Houmsi et al., 2019). Evaluating climate model experiments is a valuable approach to assessing the impacts of climate change. The latest generation of CMIP outputs (CMIP6; Eyring et al., 2016) offers a robust opportunity to re-examine past and future changes in mean and extreme climates at global and regional scales (Almazroui et al., 2021). The availability of CMIP6 GCMs allows for the exploration of potential drought hotspots by analyzing drought responses to climate change and revisiting conclusions from previous multi-model ensembles (Ayugi et al., 2022; Cao et al., 2023). These CMIP6 projections, based on improved Representative Concentration Pathways (RCPs; Van Vuuren et al., 2011) transformed into Shared Socioeconomic Pathways (SSPs; O'Neill et al., 2017), provide a suitable framework for estimating future climate variability and climate change across the MED and predicting drought. These SSPs were prominently featured in the latest IPCC Sixth Assessment Report to assess how societal actions will impact greenhouse gas emissions and the attainment of Paris Agreement targets (McBride et al., 2021). Numerous studies have already leveraged CMIP6 multi-model ensembles to investigate climate changes, consistently projecting increased intensity and frequency of extreme climates as global temperatures continue to rise (Cook et al., 2020; Almazroui et al., 2020; Almazroui et al., 2021; Li et al., 2021; Cos et al., 2022; Ayugi et al., 2022; John et al., 2022). A common approach involves utilizing the CMIP6 multi-model ensembles mean (CMIP6-MME) to mitigate uncertainty stemming from internal variability among the CMIP6 models. The CMIP6-MME has proven effective in capturing observed regional and global extreme temperature patterns (Zhai et al., 2020) and historical drought characteristics (Su et al., 2020). It also exhibits improved consistency and consensus with the most recent reference estimate for the global energy budget (Wild, 2020). Given this context, our study aims to assess and quantify future drought characteristics in Syria by analyzing projected changes in drought intensities (DIs), drought severities (DDs), and drought frequencies (DFs) using the CMIP6_MME. We will utilize the widely accepted and valuable SPI_12 and SPEI_12 indices to characterize future drought events in Syria. Using the CMIP-MME outputs from 13 CMIP6 GCMs under two SSP scenarios (SSP1–2.6 and SSP5–8.5), we will compare actual observations with model simulation outputs to evaluate their advanced capacity to capture future drought event features. This paper marks the first study of future drought characteristics in Syria using CMIP6 model outputs. The article is structured as follows: Section 2 describes the study area, climate models, and observational data, explains the methods used to correct the CMIP6 models, and presents the drought indices employed. Section 3 provides an overview of the main study results, followed by concluding remarks and avenues for further research in Section 4.

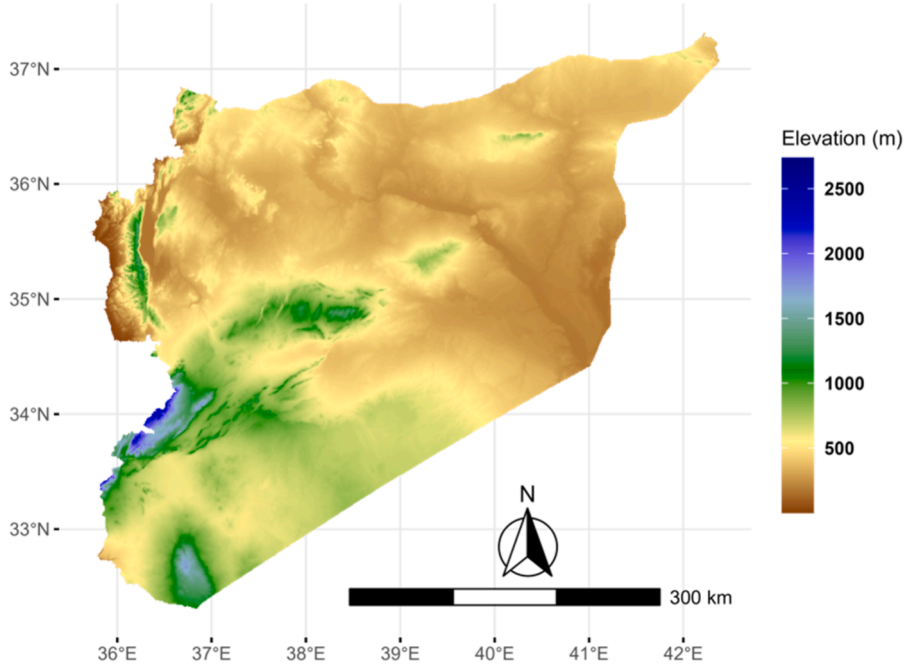

Fig. 1. Hypsometric map based on regionalized in-situ observations based on SRTM elevation data at spatial resolution of 30 s (~1 km^2).

2. Study area, data and methodology

2.1. Overview of study area

Syria is situated in the Middle East, in southwestern Asia, to the north of the Arabian Peninsula. Its geographic coordinates range between approximately 32°19′ and 37°30′ N in latitude and 35°43–37°20′ E in longitude. The country experiences a predominantly Mediterranean climate, characterized by mild, rainy winters and hot, sunny summers, with relatively humid and cold winters (Lionello et al., 2006). The most striking feature of Syria's climate is its pronounced contrast, owing to its location between the humid Mediterranean coastline and the semi-arid steppes and arid desert regions. Additionally, Syria's diverse topography, including higher elevations and steep slopes in the southwest (as depicted in Fig. 1), plays a significant role. Orographic effects in these areas can lead to increased precipitation intensity and frequency (Abou Zakhem and Hafez, 2010). The western mountainous regions of Syria are the wettest areas within the country's interior, with annual rainfall amounts exceeding 1000 mm, while the Anti-Lebanon Mountains receive over 900 mm of annual rainfall. This is partly influenced by prevailing regional atmospheric patterns originating from the northwest and moving southeast ward. The mean annual temperature in Syria varies, ranging from 7.1 °C in the mountain tops of the southwestern regions to 20.5 °C in the eastern and southeastern parts, including the deserts, where temperatures often exceed 15 °C in the coastal plain.

2.2. Observation –based data

In this study, two observational data sets downloaded on 0.5° × 0.5° resolution, have been used to consider uncertainty in observations: the observed climate parameters obtained from the University of East Anglia Climatic Research Unit (CRU TS v4.06; Harris et al. (2020) and available online at https://crudata.uea.ac.uk/cru/data/hrg/. The CRU provides a valuable resource for conducting long-term climate analyses, particularly when compared to station data. The CRU data often includes sophisticated methods for infilling missing or sparse data points, making it more suitable for continuous, long-term climate analysis (My et al., 2022). The CRU dataset has a long time series and high-quality controlled data, so it is preferred over the station data. We opted for the CRU dataset for the 1970–2000 period in Syria due to limited meteorological stations and significant gaps in precipitation records. CRU's gridded data format allowed us to interpolate and estimate missing data points, addressing these limitations. Moreover, given the current political situation, accessing up-to-date meteorological data in Syria has become increasingly challenging. Thus, relying on CRU data for this specific timeframe ensured our research's historical accuracy and relevance while navigating data collection constraints in the region. The CRU data was successfully used in several related studies (Cook et al., 2020; Papalexiou et al., 2021; Cao, 2023; Merabti et al., 2023). ERA5 reanalysis data can be accessed at https://www.ecmwf.int/en/forecasts/datasets/reanalysis and is also employed in this study. Due to its comprehensive global spatial coverage, gridded data outputs, and similarity in scale representation, ERA5 data can be more readily compared with model simulations. Even though the ERA5 data are observationally constrained model outputs, the parameters assimilated through the reanalysis prediction models are generally closer to observations (Thorarinsdottir et al., 2020). While the data spans more than seventy years, we observed anomalies such as a significant number of missing values, particularly in precipitation records, mainly affecting grids in the north and certain parts of south Syria. As a result, we chose to focus on the more recent half-century period from 1970 to 2000, during which reliable data are accessible, and studies have demonstrated the influence of warming trends on precipitation and temperature extremes (Papalexiou and Montanari, 2019). Several meteorological variables such as monthly precipitation (Pre), maximum temperature (Tmx), and minimum temperature (Tmn) are utilized for calculating the potential evapotranspiration (PET) and drought indices for the baseline period 1970–2000.

2.3. Model simulations

Historical and future climate simulations from 1970 to 2100 were extracted from CMIP6 model outputs. This study analyzes diagnostic output from 13 CMIP6-GCMs (Table 1), which are publicly available (Eyring et al., 2016; https://esgf-node.llnl.

Table 1
List of CMIP6 models used in this research along with horizontal resolution, country of origin and source reference.

CMIP 6 Model	Country	Horizontal Resolution (lon by lat in degrees)	Key Reference
ACCESS-CM2	Australia	1.3° × 1.9°	Bi et al. (2020)
ACCESS-ESM1–5	Australia	1.9° × 1.2°	Law et al. (2017)
BCC-CSM2-MR	China	1.1° × 1.1°	Wu et al. (2019)
CanESM5	Canada	2.8° × 2.8°	Swart et al. (2019)
CanESM5. CanOE	Canada	2.8° × 2.8°	Swart et al. (2019)
CMCC-ESM2	Italy	1.3° × 0.9°	Cherchi et al. (2019)
CNRM-CM6–1	France	1.4° × 1.4	Voldoire et al. (2019)
CNRM.CM6.1. HR	France	0.5° × 0.5°	Voldoire et al. (2019)
CNRM-ESM2–1	France	1.4° × 1.4°	Séférian et al. (2019)
FIO.ESM.2.0	China	1.3° × 0.9°	Song et al. (2020)
IPSL.CM6A.LR	France	2.5° × 1.3°	Lurton et al. (2020)
MIROC-ES2L	Japan	2,8° × 2.8°	Hajima et al. (2020)
MRI.ESM2.0	Japan	1.1° × 1.1°	Yukimoto et al. (2019)

gov/search/cmip6) to assess drought responses to projected climate change in Syria through the CMIP6 projections. The simulated monthly datasets of Pre, Tmx, and Tmn are evaluated for the reference period 1970–2000, while projected future changes in drought features are analyzed for the period 2015–2100 (2014 being the last year of CMIP6 historical simulations). Four future periods are considered: the near future 2015–2040, mid-future 2041–2061, 2061–2080, and the far future 2081–2100 under two SSP scenarios (SSP1–2.6 and SSP5–8.5; O'Neill et al., 2017). The historical simulations are driven by external natural and anthropogenic forcing, including volcanic eruptions, solar activity, ozone, greenhouse gases, and land-use change. Different methods for statistical and dynamical downscaling were evaluated to improve the simulations (Singh et al., 2017; Sharma et al., 2018; Zhai et al., 2020). Su et al. (2016) demonstrated that the application of statistical downscaling and bias correction to GCMs yielded reasonable and accurate results.

2.4. Model bias correction and downscaling

Our research focuses on improving the accuracy and reliability of CMIP6 data for predicting temperature and precipitation changes. To achieve this, we have chosen to utilize the non-parametric Quantile Mapping (QM) method, with a specific emphasis on incorporating robust empirical quantiles known as RQUANT. You can find a detailed explanation of this approach in Gudmundsson et al. (2012). Previous studies have highlighted the advantages of using nonparametric transformations to establish transfer functions because they eliminate the need for making specific assumptions about the initial data's distribution (Tong et al., 2021; Mondal et al., 2021; Meng et al., 2022; Dosio et al., 2022). In essence, the QM family methods aim to align historical model outputs with characteristics similar to those observed in real data. This alignment is then extended to future datasets, assuming that the bias remains consistent for both historical and projected periods, as discussed by Maraun (2013). The effectiveness of QM methods has been extensively evaluated in various studies and applied to a range of climatic variables, including precipitation, temperature, and solar radiation, across diverse geographic regions (Ayugi et al., 2021; Ngoma et al., 2021; Dike et al., 2022; Xu et al., 2022). The RQUANT method, in particular, has demonstrated its efficacy in mitigating bias in climate data when compared to various other bias correction techniques (Tong et al., 2021). It excels in replicating evaluation criteria like the Nash–Sutcliffe efficiency and mean absolute error (MAE) (Gudmundsson et al., 2012). The RQUANT method is designed to minimize the disparity between the empirical cumulative distribution functions (CDFs) of the initial model output data and those of the CRU and ERA6 observational data (Cannon et al., 2015; Tong et al., 2021; Rajulapati and Papalexiou, 2023) during a calibration period spanning from 1970 to 2000, as described in Eq. (1). After this calibration period, Eq. (2) is applied to adjust future values of the variable x for the remainder of the 21st century time series.

$$F_{m,c}(x_{m,c}) = F_{o,c}(x_{o,c}), \tag{1}$$

$$x_{b,c} = {F^{-1}}_{o,c}[F_{m,p}(x_{m,p})], \tag{2}$$

Where $x_{b,c}$ represents the outcome after bias correction; in this context, the model data is indicated by the subscript (m) where, $(x_{m,c})$and $(F_{m,c})$ represent the simulated values of the variable during the calibration period (denoted as c) and $(x_{m,p})$and $(F_{m,p})$ represent the simulated values during the projected period (denoted as p) along with their respective empirical cumulative distribution functions (F). On the other hand, $(x_{o,c})$ and $({F^{-1}}_{o,c})$ refer to the observed data (marked as o) and the corresponding inverse empirical cumulative distribution functions during the calibration period. This study utilized the QM method to disaggregate the coarse-scale climate model data to a finer spatial or temporal resolution, resulting in model outputs at a 0.5 × 0.5 resolution grid. Model corrections were executed using the qmap R package (https://cran.r-project.org/web/packages/qmap/index.html), while the downscaling process was carried out using the sdm function (https://cran.r-project.org/web/packages/sdm/index.html). This approach ensured that all datasets were standardized to a common spatial grid based on the DEM's resolution, allowing for consistent and comparable analysis. Notably, both of these methodologies employed the QM method. This combination of techniques allows for the refinement and enhancement of predictive models while also harnessing the power of the QM method to achieve more accurate and reliable results in various scientific and data analysis applications (Gudmundsson et al., 2012). The model ensemble mean, using Bayesian model averaging (BMA, as shown in Miao et al., 2014), was found to outperform other techniques in temperature simulation. Bayesian model averaging (BMA) was carried out using the BMS R package (https://cran.r-project.org/web/packages/BMS/index.html). Various statistical tests were conducted to assess the performance of CMIP6 simulations for precipitation and temperature during the baseline period, including Root Mean Square Error (RMSE), Coefficient of Correlation (CC), Nash-Sutcliffe Efficiency

Table 2
Some descriptive statistics of mean temperature and precipitation of CRU and ERA5 observational datasets and CMIP6-MME during the baseline period (1970–2000) in Syria.

Test	CRU vs CMIP6-MME		ERA5 vs CMIP6-MME	
	Temperature	Precipitation	Temperature	Precipitation
Root Mean Square Error (RMSE)	0.50	4.52	0.54	4.99
Coefficient of Correlation (CC)	0.99	0.98	0.98	0.97
Nash-Sutcliffe Efficiency Coefficient (NSE)	0.87	0.83	0.87	0.84
Mean Absolute Error (MAE)	0.40	3.47	0.44	4.63
Bias	0.01	2.04	0.03	2.01

Coefficient (NSE), Mean Absolute Error (MAE), and bias (Table 2).

2.5. Selection of drought indices: the SPI and SPEI

Drought indices are widely applied in providing a quantitative assessment of drought characteristics and risk management (Papastefanou et al., 2020). They are a very essential tool for identifying the drought dimensions and reflecting the complexity of drought-forming mechanisms and their wide range of impacts (Zhang et al., 2017; Parsons et al., 2019; Papastefanou et al., 2020; Fuentes et al., 2022). Most meteorological drought indices that use precipitation and temperature as key variables have been employed for explaining drought situations at both regional and global scales (Li et al., 2020, Xu et al., 2021) and monitoring short-term water supplies, such as soil moisture, particularly in arid and semiarid areas (Crocetti et al., 2020). Using multiple drought indices at regional and local assessment gives an actual and clearer picture of drought conditions and improves drought detection (Yang et al., 2019). In this research, the SPI (McKee et al., 1993; McKee et al., 1995) is used as purely precipitation-based drought indices. Based on data on precipitation and temperature, the SPEI (Vicente-Serrano et al., 2010) is also applied at a 12-month time scale. The use of a 12-month aggregation period usually allows inter-annual variation but it avoids the seasonal cycle (Liu et al., 2016). Moreover, it also helps in determining the possibility of droughts' persistence for long periods and considering the management of water supplies (Wu et al., 2021). In arid locales, SPI and SPEI serve as versatile tools for drought understanding and management, benefiting decision-makers like water resource managers and agricultural planners (Aadhar and Mishra, 2017). Employing both SPI and SPEI in Syria augments the precision of drought evaluation. While SPI adeptly discerns deficits in precipitation, SPEI incorporates the influential factor of evapotranspiration, amplifying our grasp of water resource availability and the gravity of drought episodes. This duality is pivotal in a region grappling with heightened water stress and climatic variability. The PET is derived using Hargreaves–Samani equation

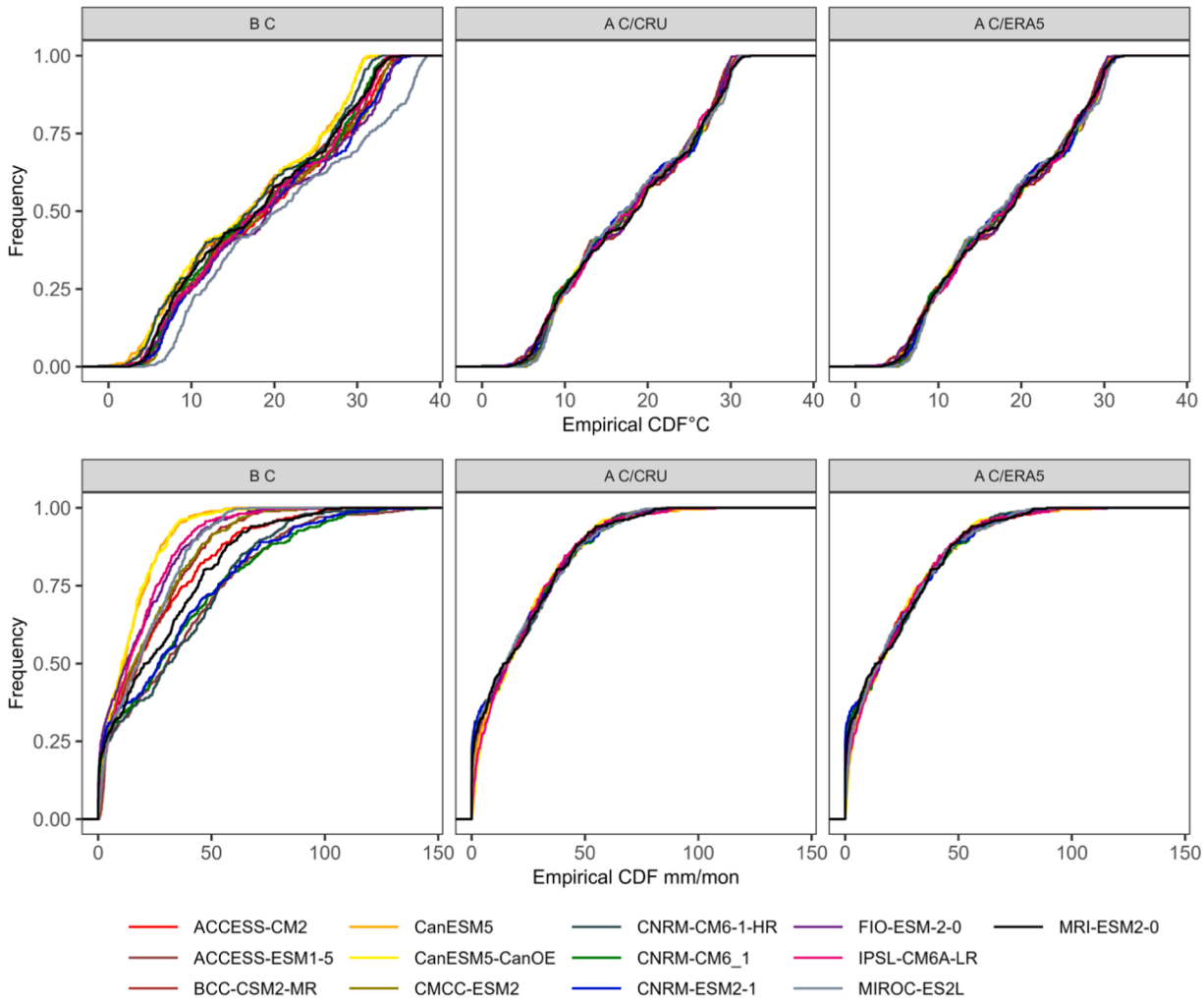

Fig. 2. Empirical cumulative density functions of CMIP models after (A) and before (B) the bias correction for temperature (upper panel) and monthly precipitation (lower panel), relative to the observations of CRU and ERA5 data1970–2000 in Syria.

(Hargreaves and Samani, 1985; Samani, 2000) that indirectly estimates extra-terrestrial radiation using both Tmax and Tmin. The Hargreaves–Samani outputs show a good agreement with the Penman-Monteith method (Beguería et al., 2014) and confirm high reliability in arid, semi-arid, Mediterranean, and very humid areas (Valipour et al., 2020). All statistical analyses are carried out in the R − 3.6.2 statistical environment (R Core Team, 2020), including ggplot2 for the graphics and maps.

2.6. Analysis of drought event characteristics

Drought duration (DD) and drought intensity (DI) are two correlated parameters commonly used to describe drought conditions (Tsakiris et al., 2016; Kwon et al., 2019; Dai et al., 2020). Drought impacts are typically determined by their duration, intensity, and frequency (Sheffield and Wood, 2011; Fung et al., 2020). To examine future changes in drought over Syria, this study considers three drought features: DD, DI, and drought frequency (DF), in order to assess the potential impacts of climate change on droughts in the context of future global warming. DD is defined as the number of consecutive months when the drought index falls below the threshold, while DI represents the average of the monthly index values per drought duration (Zhai et al., 2020). In this study, a drought event is referred to when the value of SPI_12 and SPEI_12 is equal to or less than − 1. Additionally, the frequency of drought events (DF) is defined as the number of non-consecutive drought events below our specified drought index thresholds per 100 years (McCabe et al., 2004). Further statistical analysis utilizes the Mann-Kendall test (MK) proposed by Hamed (2008) to detect trends in dryness significance and tendencies. Pearson's correlation coefficient is applied to assess the strength of a linear relationship between observations and models.

3. Results

3.1. Models correction and downscaling

The credibility of CMIP6 simulations in relation to observations hinges on their ability to accurately replicate meteorological variables, providing an overall assessment of their simulation capabilities at the country scale. To assess their performance from both temporal and spatial perspectives, simulated precipitation and temperature have been compared to observed data from the CRU and ERA5 datasets. Numerous recent studies that have employed General Circulation Models (GCMs) to predict extreme events, such as droughts, extreme precipitation, and temperature, have undertaken bias correction prior to using model outputs to evaluate projected changes across various parameters and locations (Ayugi et al., 2022; Cook et al., 2020; Ukkola et al., 2020). Fig. 2 presents CMIP6 data for monthly temperature and precipitation before (BC) and after correction (AC) when compared to the CRU and ERA5 data. The distribution of both variables exhibits strong agreement with observations after correction. The results obtained post-correction demonstrate consistent improvements across all models and broadly align with the observations provided by both datasets.

3.2. Climate parameters: evaluation of CMIP6 -MME capability in simulating historical temperature and precipitation

The ability of CMIP6 models to accurately simulate precipitation and temperature over Syria is crucial for assessing their credibility and their overall performance at the country scale. To evaluate the credibility of CMIP6 simulations in comparison to observed datasets, we compare both monthly and yearly averages to capture seasonal variations and long-term trends accurately. Additionally, we assess models from different spatial and temporal perspectives to ensure their reliability across a wide range of climate phenomena and timescales. It's important to note that CMIP6 simulations are not driven by all available historical climatic, oceanic, and boundary conditions (Meinshausen et al., 2017). Therefore, they may not fully capture the spatial and temporal variations observed in reality. To address this limitation, we focused on general statistical features (Table 1) of the simulations against observations during the baseline period (1970–2000) at different temporal scales (monthly, seasonal, annual) at the country level. Regarding precipitation, the performance of some CMIP6 models varied seasonally. In comparison to the CRU and ERA5 observational datasets, almost all CMIP6 models slightly underestimated the historical average of annual precipitation over Syria. These results suggest that the models generally reproduce the behavior of mean precipitation well in winter (DJF) and spring (MAM) but exhibit biases, particularly in simulating maximum values. Furthermore, it's worth noting that in the humid western areas of Syria, the CMIP6-MME (Multi-Model Ensemble) underestimated the variability of monthly precipitation relative to its mean. In specific details, CMIP6-MME indicated lower precipitation values in winter and spring compared to CRU and ERA5 observations. However, it overestimated precipitation in autumn and summer. In terms of temperature, most CMIP6 models reasonably captured the climatological temperature means at the country scale. CMIP6-MME was able to simulate critical temperature characteristics in line with observational data. The observed average annual temperature fell within the 5th – 95th percentile range of CMIP6-MME, indicating consistency between observational data and CMIP6-GCMs (General Circulation Models). This consistency extended to all seasons, with CMIP6-MME showing major episodic warming and cooling periods that matched observations. In summer, CMIP6-MME slightly overestimated the observed average temperature during the 1970–2000. In contrast, it tended to overestimate mean temperatures in summer and winter while underestimating autumn temperatures compared to observational datasets. In spring, CMIP6-MME demonstrated a mean temperature value consistent with historical observations, reflecting a high level of agreement. Monthly climatology plots revealed that most precipitation in Syria occurred between October and May, with peak values in January and December. CMIP6 models generally captured the climatological precipitation means well relative to observations, although they tended to underestimate monthly mean precipitation, with exceptions in May and June when CMIP6-MME exceeded observed values. These findings provide insights into the performance and limitations of CMIP6 models in simulating precipitation and temperature patterns over Syria during the historical period, aiding in

understanding their applicability for future climate projections.

The results for monthly mean air temperatures effectively represent the mean annual cycle, and the CMIP6-MME demonstrates a high degree of accuracy in capturing the observed monthly temperature variations. The discrepancies between the CMIP6-MME and observed data are minimal, with only slight overestimations of approximately 0.5 °C in June and 0.3 °C in July. In the remaining months, the differences between CMIP6-MME and both observational datasets are negligible. CMIP6 generally reports slightly higher temperatures in spring and summer but remains in close agreement with the observations. Table 2 presents various simple performance metrics used in this study to assess the quality of CMIP6-MME simulations for precipitation and temperature. The descriptive statistics affirm that the multi-year averaged monthly temperature and precipitation data from CMIP6 simulations effectively capture the principal characteristics of historical observations.

The CMIP6-MME exhibits strong correlation coefficient (CC) values between simulated and observed temperature and precipitation data in Syria. The high CC and Nash-Sutcliffe Efficiency (NSE) values, both exceeding 0.85, along with low Root Mean Square Error (RMSE) values, less than 1.0 for temperature and less than 5.0 for precipitation, underscore the CMIP6 models' capability to accurately represent observed data over Syria when considering multi-year averaged monthly time scales. To further confirm the reliability and accuracy of CMIP6 projections in representing observed data at each grid point, we present the spatial distribution of observed CRU and ERA5 data alongside the CMIP6-MME average annual temperature and precipitation in Fig. 4.

Fig. 4 illustrates that the CMIP6-MME provides highly accurate simulations of the annual temperature and precipitation dynamics across Syria. The results demonstrate that all 13 CMIP6 models closely align with both observational datasets for temperature and

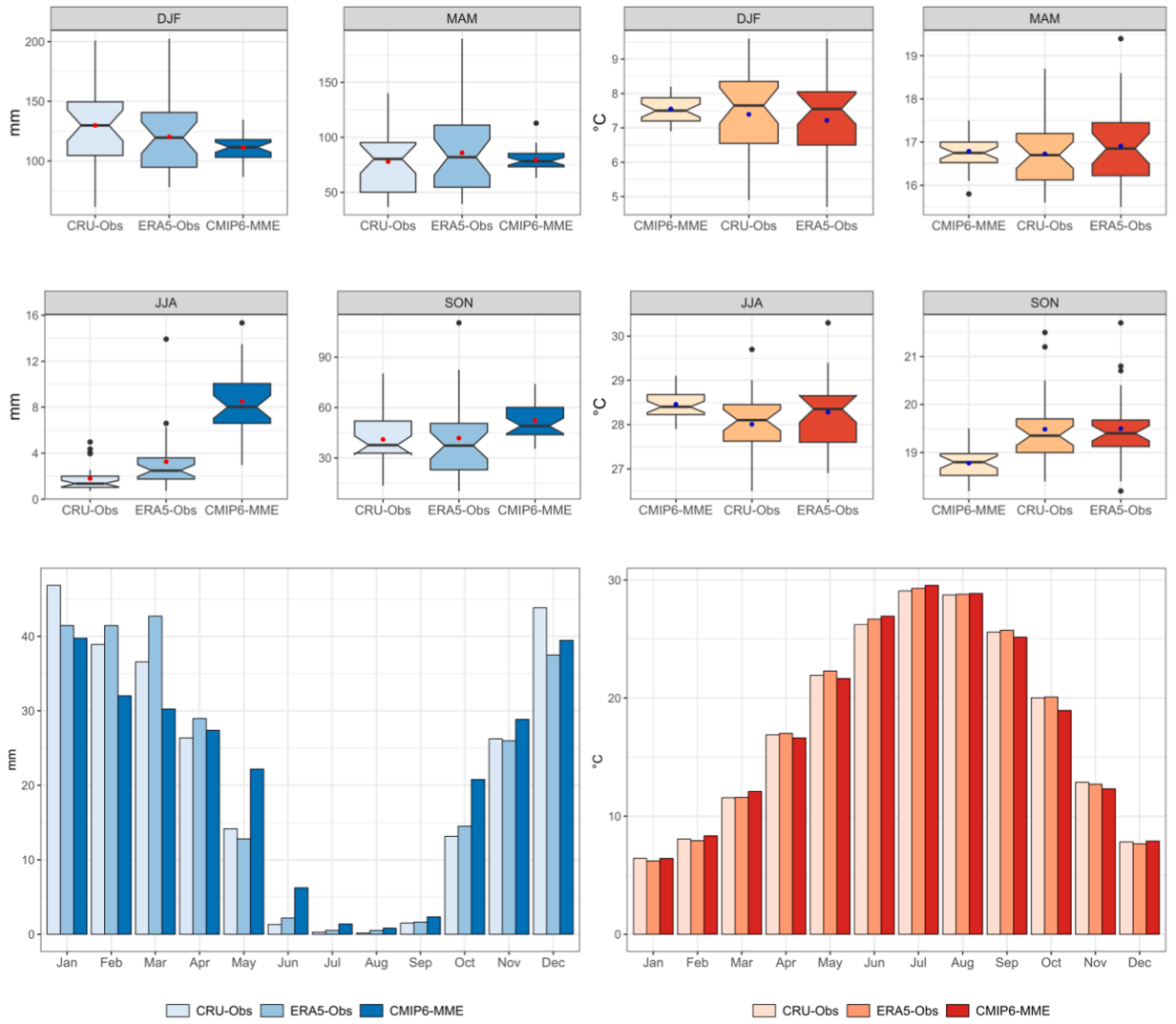

Fig. 3. Mean seasonal precipitation (upper panel-left) and mean seasonal temperature (upper panel - right). In the box, the black horizontal line represents the median and the blue dot is the mean. The upper and lower whiskers indicate the 95th and 5th percentile values, respectively. Comparison of multi-year averaged monthly Precipitation (lower panel-left) and temperature (lower panel-right) over Syria. Both precipitation and temperature data are represented by the CMIP6-MME, the CRU and ERA5 observations during 1970–2000.

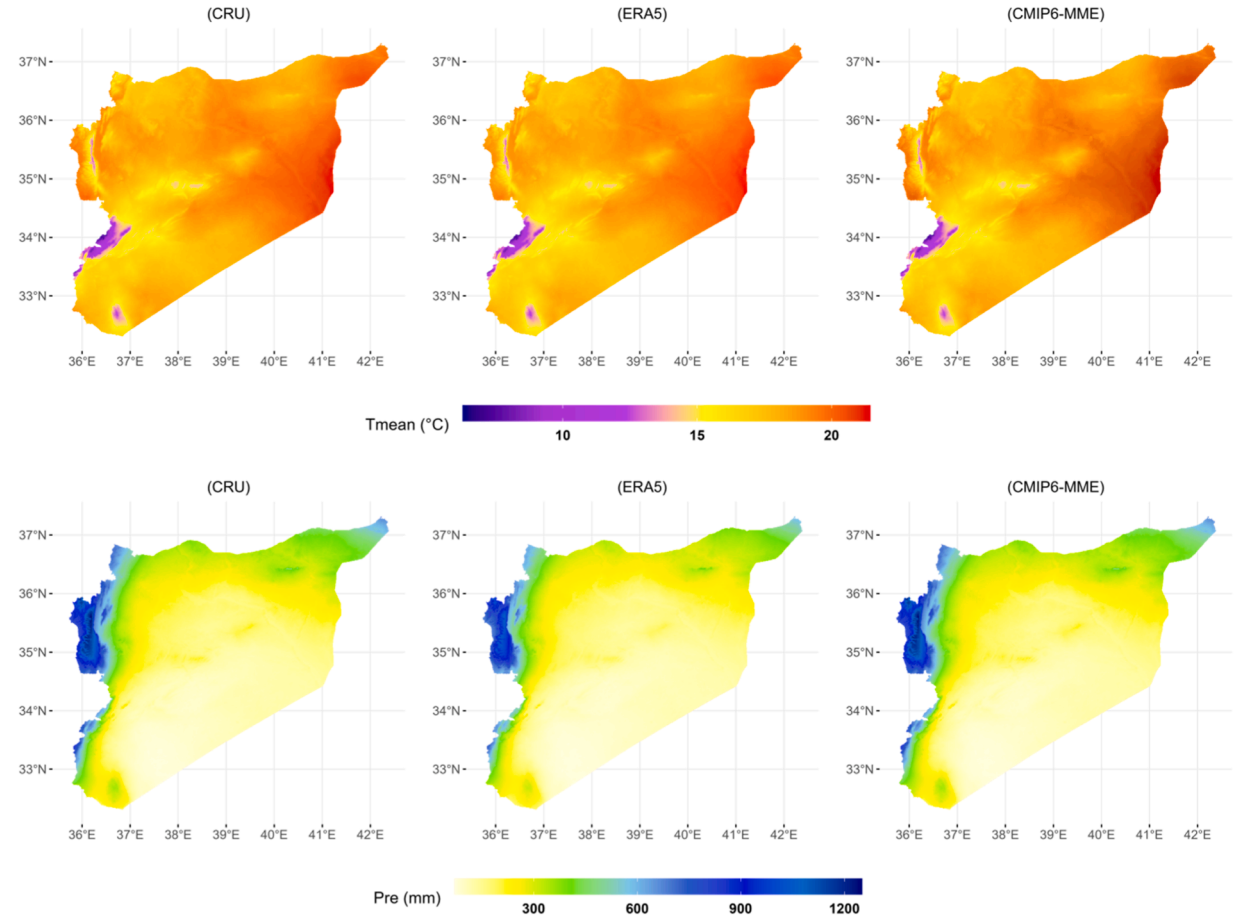

Fig. 4. Spatial distribution of mean annual temperature (upper panel) and precipitation totals (lower panel) for the baseline period (1970–2000) as based on the CRU and ERA5 observations and the CMIP6-MME.

precipitation, boasting correlation coefficients exceeding 0.95. This indicates that CMIP6 models perform exceptionally well in realistically simulating the spatial patterns of annual mean temperatures and precipitation totals in Syria. Furthermore, the CMIP6-MME effectively reproduces the distribution of annual mean temperature and precipitation totals across Syria, displaying less bias compared to the CRU dataset than the ERA5 observational data. Fig. 4 clearly illustrates that the CMIP6-MME successfully captures the spatial patterns of annual mean temperatures over Syria. The lowest temperatures are recorded in the Anti-Lebanon Mountains in southwest Syria, while the highest values are observed in the eastern and northeastern regions of Syria. The distinct precipitation patterns, as portrayed by the CMIP-MME and both observational datasets, highlight that the mountain range parallel to the coast in the west and the Anti-Lebanon Mountains in the southwest are the wettest areas in Syria.

3.3. Drought features: evaluation of CMIP6 -MME capability in simulating historical drought events characteristics

Utilizing monthly temperature and precipitation data from CMIP6-MME, as well as data from both the CRU and ERA5 observational datasets, we computed SPI_12 and SPEI_12 indices during the baseline period (1970–2000). These indices were used to assess drought characteristics at various spatial and temporal scales in Syria. Fig. 5 presents the evolution of the sum of monthly drought severities for each year and the percentage frequency of different SPI_12 and SPEI_12 classification classes across Syria. It is evident that there is a high level of agreement in the inter-annual variability of SPI_12 and SPEI_12 between the CMIP6-MME and both observational datasets, revealing a consistent downward trend in observed and simulated historical data. The CMIP6-MME successfully captured the progression of wet and dry years, although its performance was more accurate when compared to the CRU dataset than the ERA5 climatology. Notably, the CMIP6-MME effectively represented major historical dry and wet years in Syria. Furthermore, it accurately depicted extreme drought events that occurred in the 1990 s, which featured extended drought periods ranging from 15 to 20 months according to SPI_12 and 27–29 months according to SPEI_12.

The ability of CMIP6 models to simulate the spatial patterns of DI, DF, and mean drought duration (MDD) across each grid point in Syria was also assessed in comparison to observational data. In general, the CMIP6-MME demonstrated a high level of proficiency in identifying drought events, and its performance was consistent with both the CRU and ERA5 observed datasets during the baseline

Fig. 5. Temporal variation of historical SPI_12 and SPEI_12 values (upper panel) at a country level. The grey line or regression line represents a smoother (mean annual SPI_12 and SPEI_12 values for each year). The historical mean drought duration for 30-yr (middle panel) period. Frequency of time (%) in each dry and wet category (lower panel). Graphs are built on the historical observed CRU, ERA6 and simulated CMIP-6-MME data and all drought features are built on the SPI_12 and SPEI_12 values.

period. This indicates a strong agreement in representing the spatial distribution of DI, MDD, and DF, as illustrated in Fig. 6(a, b, c).

Overall, CMIP6 simulations demonstrated a high level of accuracy in identifying drought events when compared to both the CRU and ERA5 observational datasets. The CMIP6-MME exhibited very similar spatial patterns of DI values to the CRU and ERA5 observational data for both SPI_12 and SPEI_12, with a slight overestimation of DD for the SPEI_12, as depicted in Fig. 6(a). According to both drought indices, many regions across Syria had relatively low average DI values (<-1.5) during the baseline period, a pattern consistent in both observed and simulated historical data. When using SPEI_12, the most intense drought events primarily occurred in northern and northeastern Syria, while central and southwestern regions experienced significant drought events during the baseline period (1970–2000) according to SPI_12. Additionally, we assessed the ability of CMIP6 to replicate the spatial patterns of MDD, as shown in Fig. 6(b). Drought duration plays a crucial role in determining the onset and cessation of each drought event. To further assess the reliability of CMIP6-MME across each grid point, we examined the spatial distribution of DD based on the observation (CRU and ERA5) and simulations (CMIP6) for the baseline period (1970–2000).

During the period from 1970 to 2000, CMIP6 models effectively captured observed drought durations (DD) for both SPI-12 and SPEI_12. The spatial pattern of DD in CMIP6 simulations closely resembled that of the observed data for both SPI_12 and SPEI_12. In terms of accuracy, the CMIP6-simulated DD closely matched the CRU and ERA5 observations, achieving approximately 95% agreement for DD durations ranging from 5 to 9 months with SPI_12 across all grid points, and around 93% for SPEI_12. However, it's worth noting that CMIP6 simulations exhibited an overestimation of DD patterns in eastern Syria, while the southwestern region showed a slight underestimation of DDs, with the maximum discrepancy being 7.8 months. In contrast, both CRU and ERA observations indicated longer DD durations, measuring 9.6 and 10.1 months, respectively. Based on SPI_12, the longest drought events were predominantly observed in the east and southwest parts of Syria, while SPEI_12 indicated the longest dry periods in the east and northeast

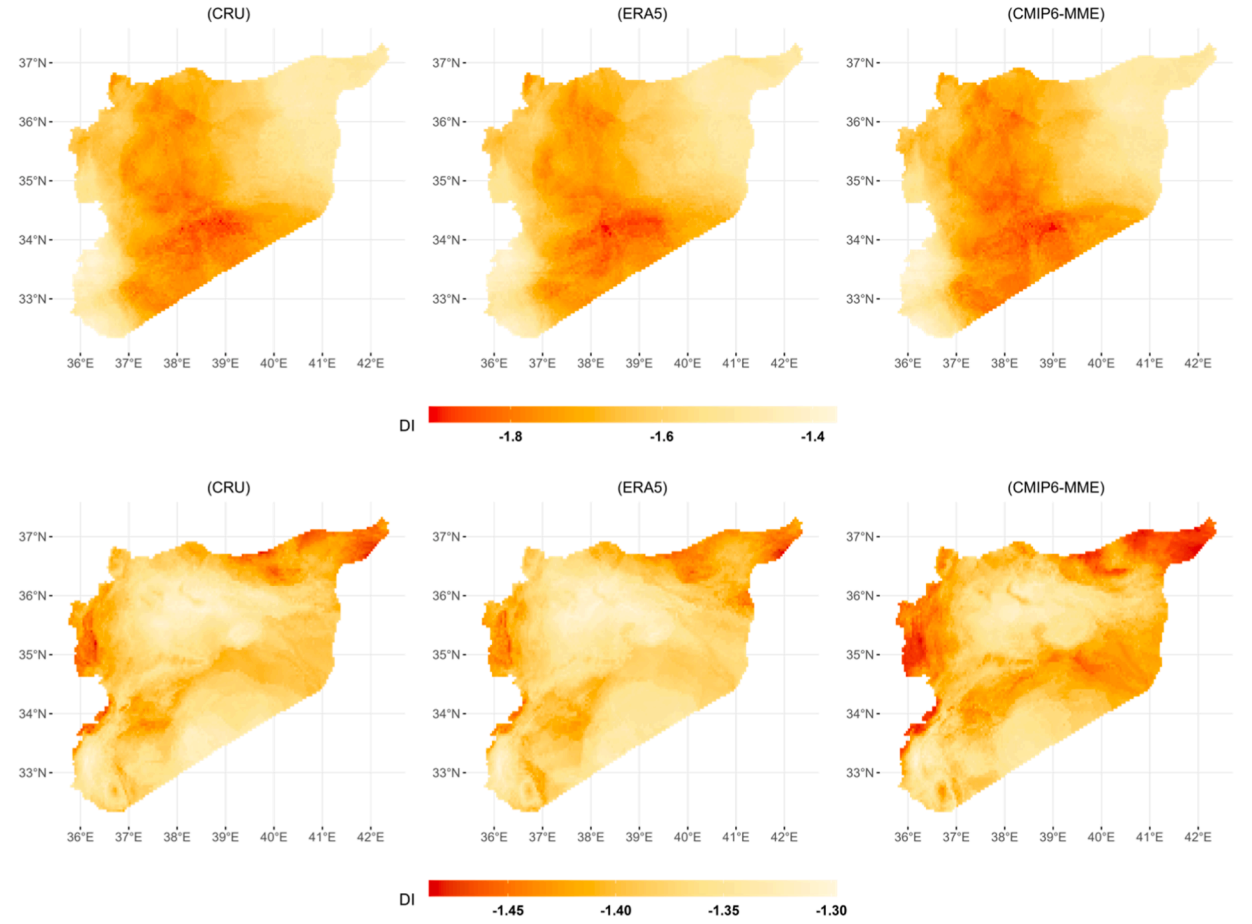

Fig. 6. (a). Spatial pattern of average Drought Intensity (DI) obtained by the SPI_12 (upper panel) and the SPEI_12 (lower pannel) calculated from the CRU and ERA5 observations, and simulations (CMIP6-MME) for the baseline period (1970–2000) across syria. (b). Spatial patterns of the MDD obtained by the SPI_12 (upper panel) and the SPEI_12 (lower pannel) calculated from the CRU and ERA5 observations, and simulations (CMIP6-MME) for the baseline period (1970–2000) across syria. (c). Spatial pattern of average Drought Frequency (DF) obtained by the SPI_12 (upper panel) and the SPEI_12 (lower pannel) calculated from the CRU and ERA5 observations, and simulations (CMIP6-MME) for the baseline period (1970–2000) across syria.

regions. The spatial distribution of Drought Frequency (DF) from CRU, ERA5, and CMIP6-MME exhibited similar patterns across Syria. DF based on SPI_12 displayed high values (>15%) in most of Syria, with the northeast experiencing the highest occurrence (as shown in Fig. 6-c). Similarly, the highest DF values (>15% for SPEI_12) were prevalent in many parts of western, southwest, southern, and central Syria. CMIP6-MME successfully detected these observed DF patterns for both SPI_12 and SPEI_12 during the baseline period (1970–2000).

3.4. Projected changes in temperature and precipitation across the SSPs scenarios in Syria

Drought conditions are typically exacerbated by rising temperatures and declining precipitation. Therefore, we conducted a detailed analysis of the spatial and temporal changes in projected temperature and precipitation in Syria. Compared to the baseline period of 1970–2000, the temperature projections from various CMIP6 models indicate a significant increase in warming over Syria under both future scenarios (SSP1–2.6 and SSP5–8.5) throughout the entire simulation period from 1970 to 2100 (Fig. 7-a; left panel).

Under both scenarios (SSP1–2.6 and SSP5–8.5), there are strong and significant projections of warming throughout the 21st century, with the most pronounced temperature increases expected by 2050 and beyond, particularly under the high-emission scenario (SSP5–8.5). The temperature projections begin to diverge noticeably after 2050, mainly due to differences in emissions trajectories. The SSP5–8.5 scenario exhibits the most substantial warming trend, with temperatures expected to exceed a 4.5 °C increase by the latter part of the 21st century, translating to a warming rate of 0.8 °C per decade from 2015 to 2100. Even under the more aggressive mitigation scenario SSP1–2.6, there are projected temperature increases, though they are less pronounced, with a projected increase of 2.1 °C by 2100. When examining seasonal variations, the warming trends in winter and spring are milder compared to those in autumn

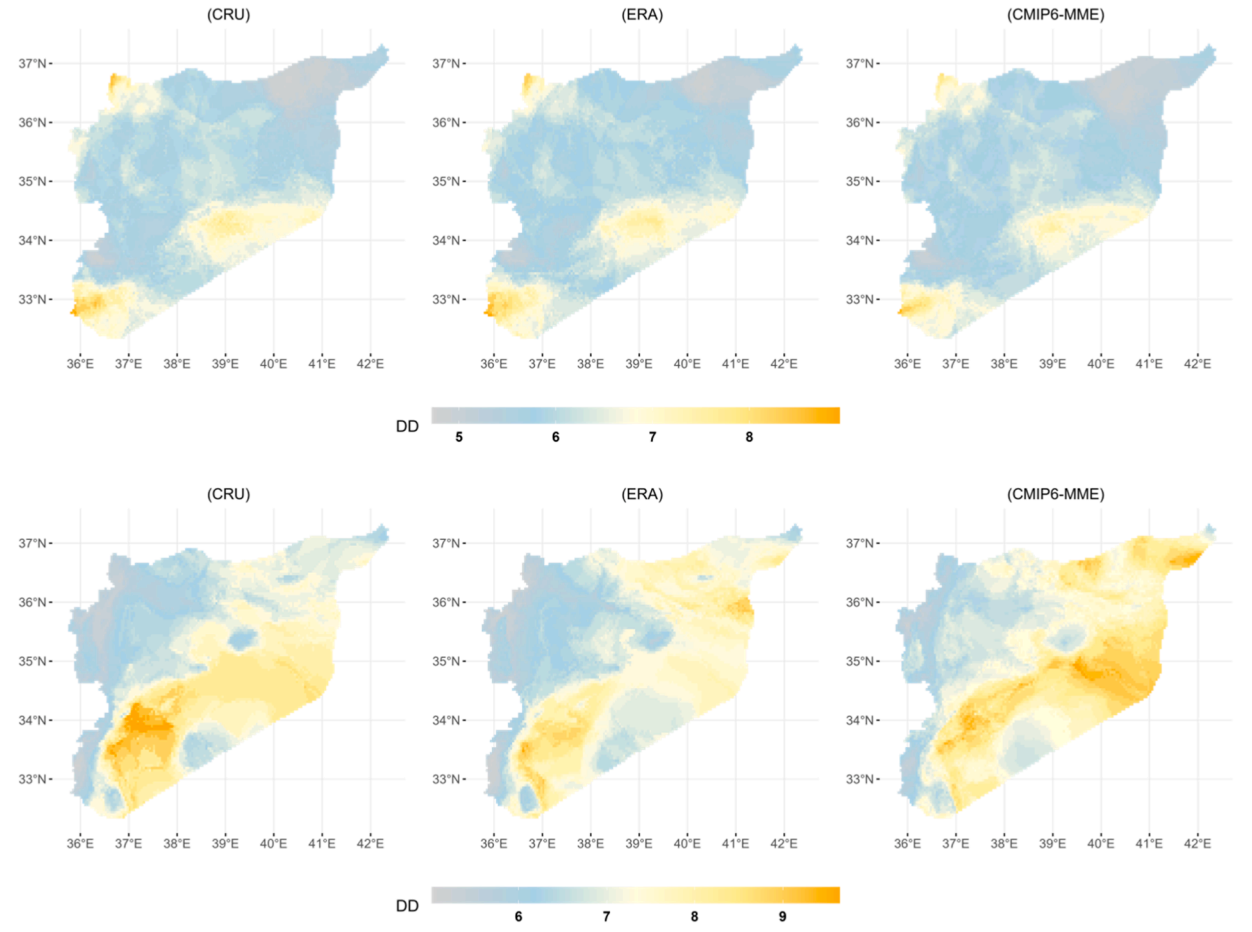

Fig. 6. (*continued*).

and summer. Among the seasons, the highest amplified warming is observed in JJA (June, July, August) relative to the 1970–2000 seasonal mean. By the end of the century, CMIP6 simulations indicate a mean summer (JJA) temperature that is 5.7 °C higher than that in the reference period, with a warming trend of 0.95 °C per decade under SSP5–8.5 and 0.15 °C per decade under SSP1–2.6 during 2015–2099. For MAM (March, April, May), CMIP6 projects a mean warming of 2.4 °C and 4.1 °C relative to the baseline period under SSP1–2.6 and SSP5–8.5, respectively. In contrast, the magnitude of warming amplification in DJF (December, January, and February) is comparatively small and is not expected to exceed 2.0 °C under the high-emission scenario SSP5–8.5. Additionally, there is a downward trend in annual mean precipitation (Fig. 7-B-right) projected under both scenarios. However, this trend levels off under the high mitigation scenario, SSP1–2.6, as the climate stabilizes later in the 21st century. The anticipated future precipitation deficit in Syria is primarily due to decreased precipitation in DJF and MAM, which intensifies as radiative forcing increases.

Under both the SSP1–2.6 and SSP5–8.5 scenarios, there are projected reductions in winter rainfall in the far future (2081–2100) compared to the reference period. In this period, rainfall is expected to decrease by 26.8 mm (a 23.0% reduction) under SSP1–2.6 and 27.7 mm (a 23.8% reduction) under SSP5–8.5. Conversely, a substantial increase in mean summer rainfall is projected over the course of the 21st century, with values ranging from 10.5 mm to 11.3 mm, representing a significant increase of 147.1–151.6% under SSP5–8.5 and SSP1–2.6, respectively. Furthermore, a robust increase in mean autumn rainfall is anticipated across Syria. The most significant performance increases, amounting to approximately 9.5 mm (a 20.2% increase), are expected in the near-term future, particularly in 2033, 2039, and 2040, under the high greenhouse gas emissions scenario (SSP5–8.5), relative to the reference period (1970–2000). The CMIP6-MME future projection anomalies of surface temperature at the annual scale are illustrated for the short-term (2021–2040), mid-term (2041–2060, 2061–2080), and far-term (2081–2100) periods under the SSP5–8.5 forcing scenario, taking into account the baseline period of 1970–2000 (Fig. 8. a).

The spatial anomalies of temperature change during 2021–2100 display consistent patterns of change under both selected emission scenarios. These patterns show that differences in temperature change become more pronounced from the mid to the far future, while the spatial pattern remains consistent, indicating the highest positive anomalies in northern and northeastern Syria. According to the CMIP6-MME ensemble mean annual temperature, projected warming across Syria is not uniform and exhibits regional variations, ranging between 1.4 °C and 3.5 °C. Under the SSP5–8.5 scenario, there is a substantial additional warming of mean surface air temperature, exceeding 7.5 °C by the end of the 21st century. In contrast, the high-mitigation scenario (SSP1–2.6) limits surface

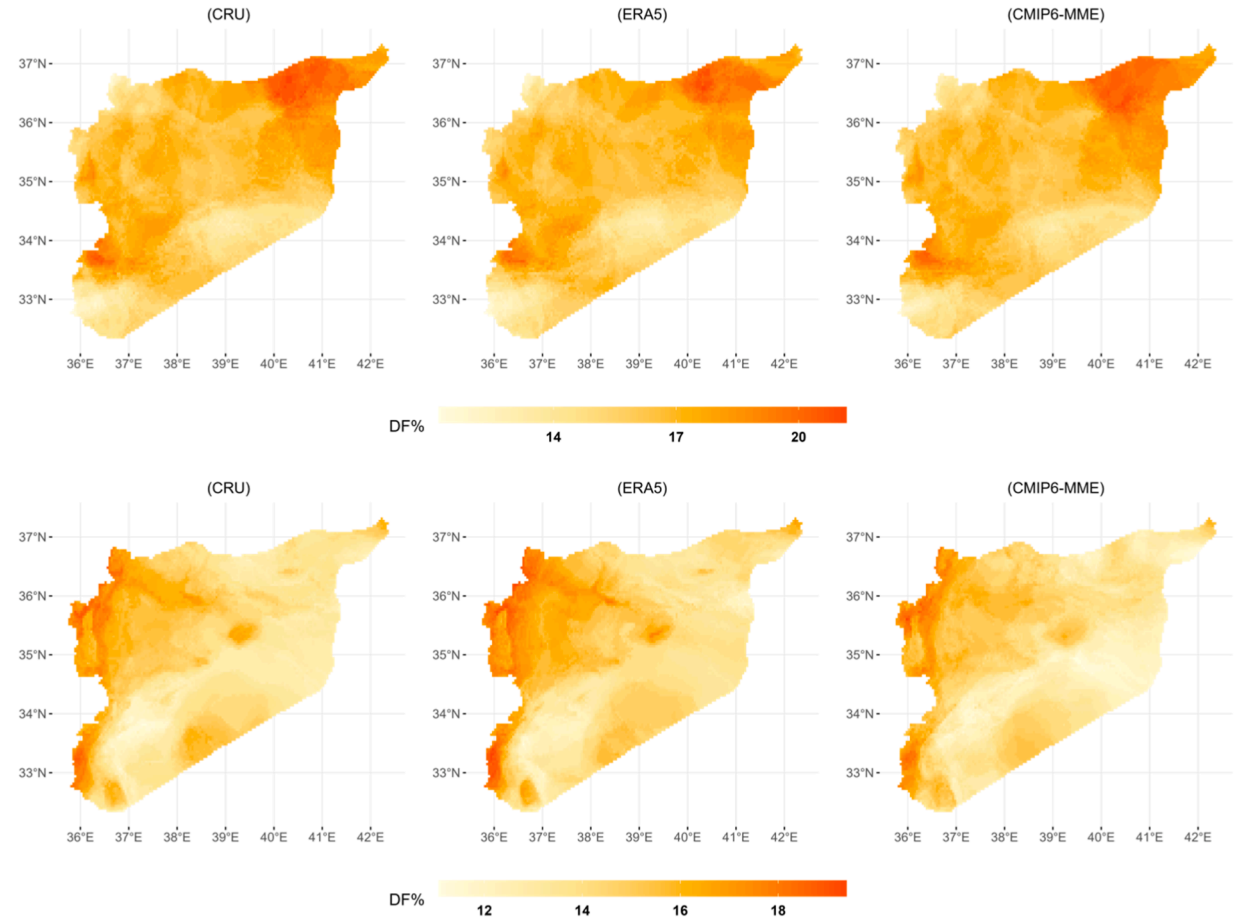

Fig. 6. (*continued*).

warming to 3.5 °C. The spatial distribution of annual precipitation anomalies, derived from downscaled CMIP6-MME scenarios and compared to the baseline period (1970–2000), is illustrated in Fig. 7. b. Precipitation change patterns over Syria become more robust and significant over time, and the CMIP6-MME from 13 models effectively captures the spatial patterns of future annual precipitation changes. Across the four future periods, a consistent pattern emerges, with a general negative anomaly indicating increased dryness over Syria. This dryness is more pronounced under the high-emission scenario (SSP5–8.5), suggesting a clear shift toward drier conditions in central, western, northern, and northeastern Syria.

3.5. Projections in the main drought characteristics over Syria

3.5.1. Projected change in drought intensity (DI) in Syria

Drought Event Intensity (DI) is a commonly used metric to gauge the overall intensity of drought events. In this study, DI was calculated as the 30-year average of all event-average SPI-12 and SPEI_12 values at each grid cell for each period, averaged over all models. The results indicate that both SPI-12 and SPEI_12 are expected to exhibit more significant negative oscillations under the SSP5–8.5 scenario, particularly towards the latter part of the 21st century (see Fig. S1). The research also examined drought intensity based on CMIP6-MME for all future periods under both scenarios to assess how the spatial and temporal distributions of DIs have changed due to ongoing warming and how they may evolve in the future in Syria. Overall, there is a projected increase in dryness in the future under both scenarios, with a more pronounced trend under the high-emission scenario, SSP5–8.5. According to SPEI_12, drought conditions are expected to become more severe and intensify further in the 2060 s under SSP5–8.5, while SPI_12 suggests oscillations around zero in the near and mid-future (2015–2060). Using a 12-month time scale, it is observed that moist and drought periods exhibit lower temporal frequency and longer duration (see Fig. S1). As the 21st century progresses, differences in DIs determined by SPI_12 may become minimal, with slightly higher intensity projected in the mid-future, particularly in the mid-2070 s under the SSP5–8.5 forcing scenario. Compared to the historical period, a larger intensification of droughts is predicted by SPEI_12 under both scenarios starting in the 2060 s, indicating that drought evolution will be primarily driven by temperature. Based on SPI_12 and SPEI_12, certain regions of Syria may experience severe droughts in the early and mid-future, followed by more vigorous growth in the 2060 s under SSP1–2.6. Robust dryness is projected over the entire country under both scenarios, with variations in spatial

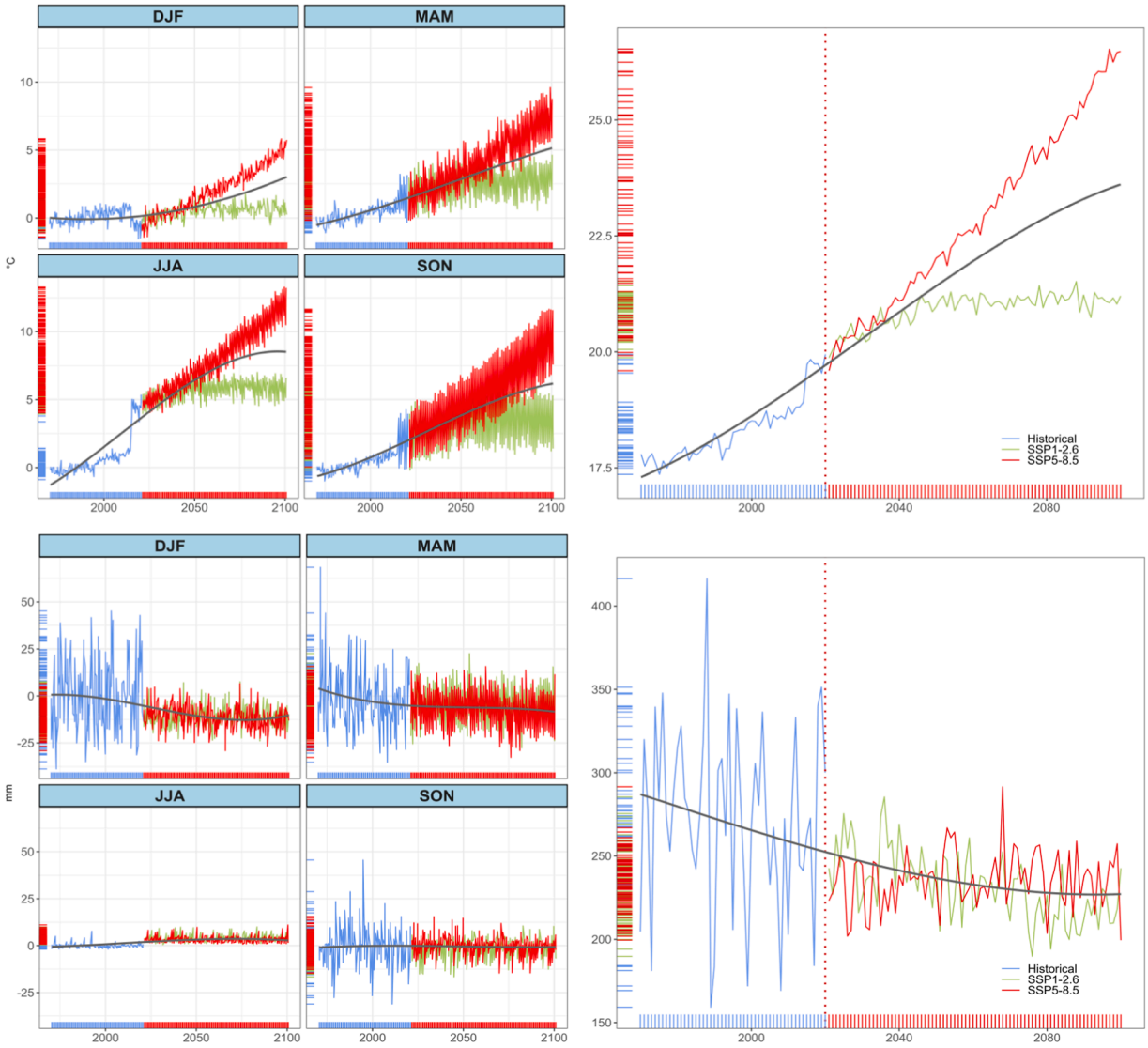

Fig. 7. **a**.Temporal changes in the monthly mean temperature relative to the reference period (19,070–20,00) for each season (left panel). CMIP6-MME simulations time series for baseline period (1970–2000; blue) and under SSP1–2.6 (green) and SSP5–8.5 (red) forcing scenarios (right panel). The grey line or regression line represents a smoother mean annual values for each year. **b**.Temporal changes in the monthly precipitation relative to the reference period (19,070–20,00) for each season (left panel). CMIP6-MME simulations time series for baseline period (1970–2000; blue) and under SSP1–2.6 (green) and SSP5–8.5 (red) forcing scenarios (right panel). The grey line or regression line represents a smoother mean annual values for each year.

distribution between the two scenarios. Consequently, future drought conditions are expected to dramatically increase in the western coastline and southern regions, with the most pronounced drying by 2100 under SSP5.5.8. The changes in DIs indicated by SPEI_12 suggest a clear trend towards dryness in several areas; with some differences in spatial patterns compared to those indicated by SPI_12 (see Fig. S2). Therefore, considering the impact of warming, it is anticipated that Syria will experience increasingly drier periods. There is a rising likelihood of droughts occurring across most parts of Syria, with the SPEI_12 analysis suggesting that extreme dry conditions may occur several times per decade by 2100. These findings align with the conclusions of Zhong et al. (2020) and Mathbout et al. (2021), highlighting the greater effectiveness of temperature-based indices in assessing drought conditions compared to purely precipitation-based indices. However, the spatial patterns of DIs indicated by both drought indices are projected to increase from the 2060 s onwards. According to both indices, CMIP6 simulations project a potential tripling in the area that might experience severe to extreme meteorological droughts in Syria under the SSP5–8.5 scenario by 2100. It's worth noting that the underestimation of monthly precipitation variability relative to its mean in humid areas of Syria could impact the projected drought intensities (DIs), as accurately capturing DIs requires skillful simulation of both mean precipitation and its variability (Ukkola et al., 2018).

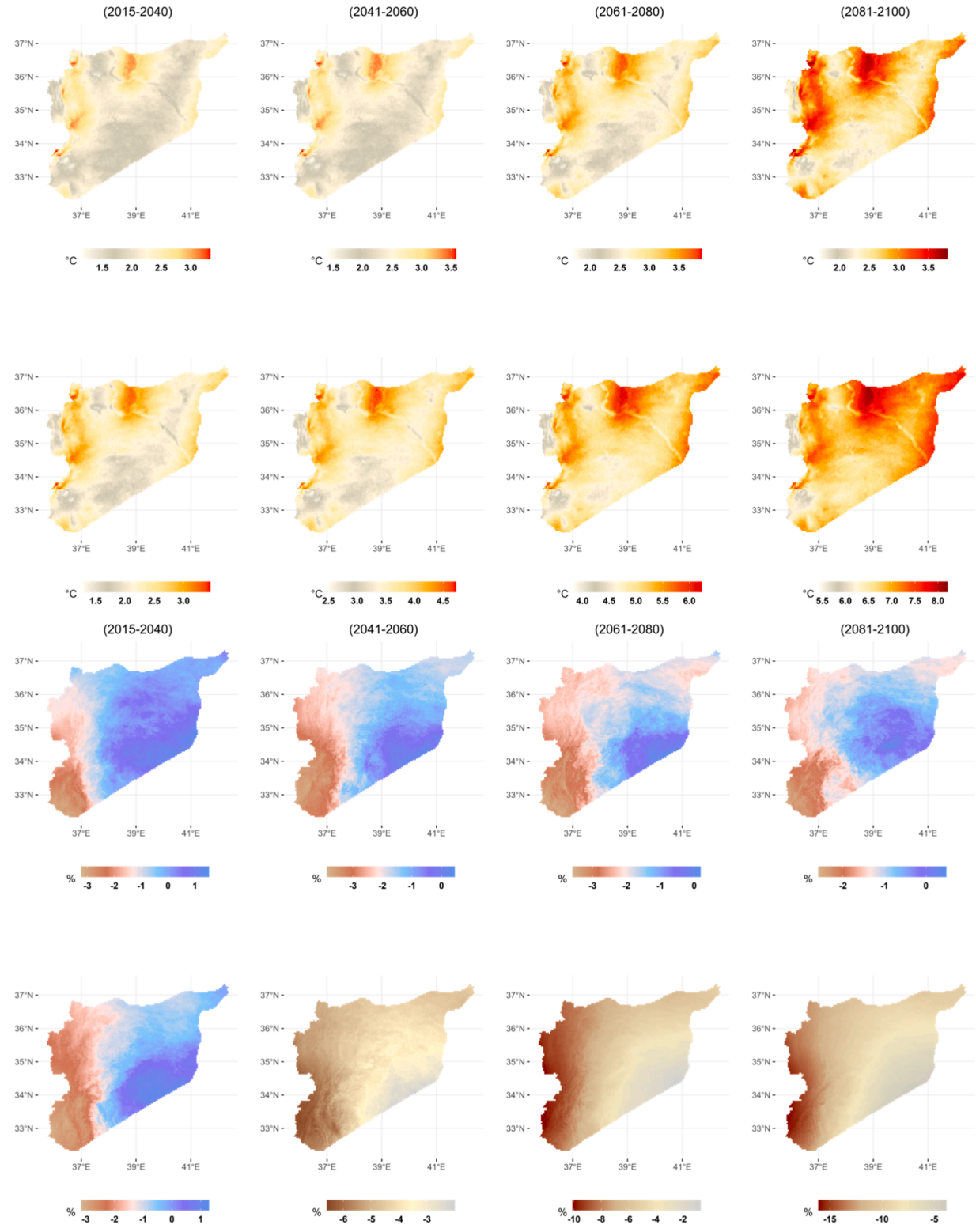

Fig. 8. **a** Spatial patterns of changes of CMIP6-MME ensemble mean annual temperature under the SPP1–2.6 (upper panel) and under the SPP5–8.5 (lower panel) forcing scenarios for near, mid and far future periods relative to baseline period (1970–2000). **b** Spatial patterns of changes of CMIP6-MME ensemble annual precipitation under the SPP1–2.6 (upper panel) and under the SPP5–8.5 (lower panel) forcing scenarios for near, mid and far future periods relative to baseline period (1970–2000).

3.5.2. Projected change in drought duration (DD) and drought frequency (DF) in Syria

The projected changes in Mean Drought Duration (MDD) for severe or extreme droughts are examined at the country level using CMIP6-MME under both low and high-emission scenarios, based on SPI_12 and SPEI_12. The shifts in average and maximum drought durations according to these two indices are depicted in Fig. S3. Overall, Syria is expected to undergo drought events with prolonged durations in the future under both forcing scenarios. Furthermore, under the SSP5–8.5 scenario, the SPI_12 projects longer MDDs in the mid-future, estimated at 7.3 months and 17.1 months for the periods 2041–2060 and 2061–2080, respectively. However, for the SSP585 scenario, the SPI_12 exhibits lower skill in capturing observed drought durations in Syria by the late future. In contrast, the MDD constructed by the SPEI_12 is projected to reach 47.6 months with a maximum duration of 80 months by the end of the 21st century (2081–2100). Since the 2060 s, the estimated MDD is 5.1 months, and the intensity of drought is 2.1 times higher than in the reference period. Notably, under the SSP585 scenario, regions that are already arid, particularly in eastern and northeastern Syria, may become severely affected by drought by the late 21st century (see Fig. S3). As observed, the inland areas, forming the dry zone, are expected to experience drought events with longer durations under the high-emissions scenario (SSP5–8.5). In contrast, shorter drought events may be reported along the coastal line in the west and in the mountainous regions in the southwest. It is worth noting that, under the high-emission SSP and based on SPEI_12, Syria is projected to experience its longest dry events by the end of the century, exceeding 40 months in the eastern and northeastern parts. For both scenarios, MDDs are expected to mostly increase from the 2060 s onwards. This increase is also evident in the low-emission scenario, projected to start in the 2040 s and reach up to 13 months based on SPEI_12 (see Table 3). These findings indicate that by the late 21st century, MDD will be 5.1 times longer under the SSP585 pathway compared to the historical reference period (1970–2000).

With higher emissions, the highest Mean Drought Duration (MDD) is projected to increase by 41 months under SSP5–8.5 based on SPEI-12 over Syria, particularly in the eastern and northeastern parts (see Fig.S3). Conversely, in the early future, a slight decrease in MDD is estimated, by 0.5 and 2.5 months according to SPI_12 and SPEI_12, respectively, compared to the baseline period of 1970–2000. These regions are expected to face a high risk of drought under high-emission scenarios. Notably, across various scenarios, regions, and future periods, Syria is likely to experience longer dry periods under high-emission scenarios. To gain further insight into the frequency of droughts in Syria, an examination of drought frequency was conducted. Drought frequency based on SPI_12 and SPEI_12 is expected to noticeably increase in the late future under both scenarios. Here, changes in Drought Frequencies (DFs) using SPI_12 and SPEI_12 for future periods (2015–2100) are compared to the baseline (1970–2000). According to SPI_12, the frequency of extreme and severe droughts is projected to decrease by 1.2% and 2.1% under SSP5–8.5. In contrast, severe droughts, based on SPEI_12, are expected to increase by 3.5% under the same forcing scenario, indicating a significant response of drought to future temperature changes (see Fig. 9).

Under the high mitigation scenario (SSP1–2.6), the Drought Frequencies (DFs) driven by the SPEI_12 show a reduction in occurrence by 2.9%, which can be attributed to temperature stabilization or even a slight decline in the second half of the 21st century under this scenario (as suggested by Tebaldi et al., 2021). It's noteworthy that less frequent droughts are projected in Syria under both scenarios. This change is a consequence of the projected shift from short-term drought events to long-term drought events in the country. In general, the frequency of drought events in Syria is expected to decrease during the periods 2021–2060 and 2061–2100 according to both SPI_12 and SPEI_12. For the future period of 2061–2100, the average drought event frequency in Syria is estimated to be about 8.1 and 5.5 events (an average of all scenarios) using SPI_12 and SPEI_12, respectively. These values are lower than the averages recorded in the baseline period (14 and 9 events), respectively. Consequently, the frequency of drought events in Syria is projected to be lower relative to the reference period. However, it's important to note that the duration of drought events (DD) and their intensities (DIs) are expected to increase, leading to the emergence of stronger droughts in Syria. When comparing different Shared Socioeconomic Pathways (SSPs) in terms of the impact of emissions, lower drought event frequencies correspond to higher-emission scenarios. This relationship is most prominent during the near and mid-future periods and is especially pronounced for drought events driven by the SPEI_12, with frequencies of 4.1 and 1.7 events under SSP1–2.6 and SSP5–8.5, respectively. Combined with the earlier analysis of drought characteristics, these findings further indicate that drought spells in Syria will transform into long-term drought events under high-emission SSPs.

4. Discussion and conclusion

This research explores the forecasting of drought attributes in Syria, specifically examining their duration, frequency, and intensity. It employs an ensemble of 13 models derived from the most recent CMIP6 dataset, encompassing two different SSPs scenarios. To assess CMIP6's effectiveness in representing drought features in Syria, the study compares it to observed monthly climate data from CRU TS v4.06 and ERA 5, alongside the CMIP6 model ensemble outputs during the reference period (1970–2000). The chosen ensemble from CMIP6 exhibits a strong ability to replicate current climate parameters such as precipitation and temperature, while also effectively reproducing drought characteristics within Syria. The majority of CMIP6 models exhibited an underestimation of average winter and spring precipitation. Nevertheless, CMIP6-MME effectively replicates the general decline observed in seasonal and annual precipitation. Throughout the baseline period, Syria experienced prevalent high temperatures and low precipitation, especially in its arid and semi-arid regions situated in the central, eastern, and northeastern areas. In terms of spatial representation, the CMIP6-MME accurately mirrors the geographical patterns of precipitation and temperature in Syria. In the future, temperatures in north, east, and northeast Syria will rise significantly. Although there are uncertainties in projecting precipitation changes using CMIP6 data, this study effectively highlights decreasing rainfall patterns across Syria, especially in the southwest (Anti-Lebanon Mountains). Temperature projections indicate a consistent warming trend in Syria, with a noteworthy increase in magnitude as we move from the mid to the distant future. Overall, the anticipated shifts in both precipitation and temperature in Syria progress monotonically from the

Table 3
Differences (in months) of MDDs between near, mid, and late future periods and the reference period (1970–2000) over Syria under the SSP1–2.5 and the SSP5–8.5 forcing scenarios.

Period	SPI_12		SPEI_12	
	SSP1-2.6	SSP5-8.5	SSP1-2.6	SSP5-8.5
2015–2040	2	-3	-3	-2
2041–2060	2	1	2	-2
2061–2080	3	11	13	2
2081–2100	1	5	5	41

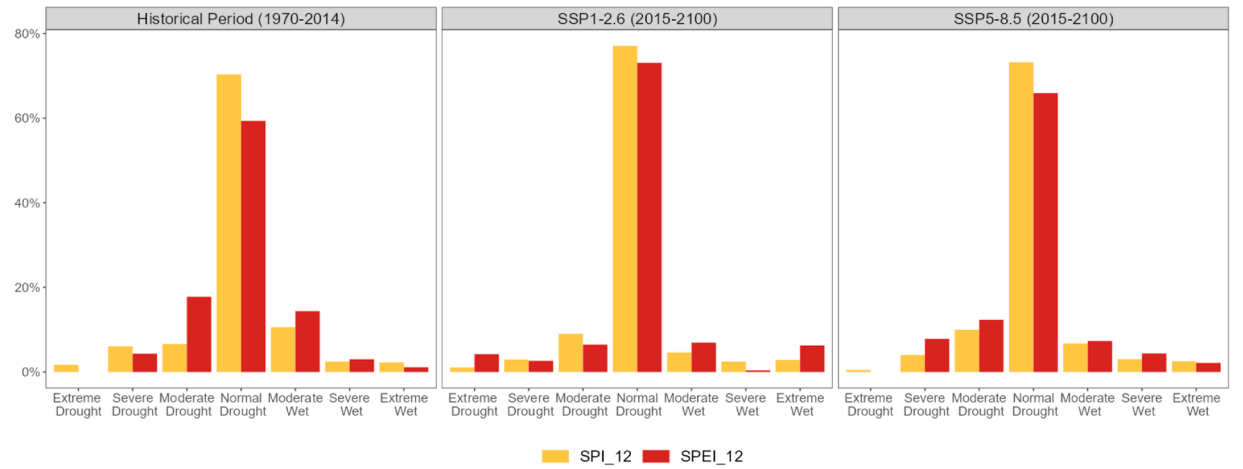

Fig. 9. Frequency of time (%) in each dry and wet category of SPI_12 and SPEI_12 for historical (1970–2020), reference (1970–2000), and future (2015–2100) periods in Syria..

mildest (SSP1–2.6) to the most severe (SSP5–8.5) scenarios and from the mid-term (2041–2070) to the late-term (2081–2100) projection periods. The anticipated shifts in temperature and precipitation are reflected in changes in drought characteristics as indicated by drought indices. Projections based on SPI_12 and SPEI_12 show that drought conditions will worsen, becoming more severe, intense, and prolonged. Both indices predict more intense drought events with longer durations and greater intensities in the eastern and northeastern regions. In summary, under a high-emission scenario (SSP5–8.5), these areas are at significant risk of experiencing severe drought conditions. The most prominent patterns of severe drought conditions (DIs and DDs) consistently appear in Syria's arid and semi-arid eastern and northeastern regions for both indices. The CMIP6 simulation shows a clear overestimation of both DIs and DDs derived from SPEI_12, primarily because of the overestimation of temperature and, consequently, PET. Overestimated CMIP6 drought projections, due to high-temperature estimates, can misguide policymakers in arid regions like Syria. Relying on exaggerated models can lead to misallocated resources, delayed responses to actual droughts, and hindered adaptation efforts to mitigate the impact of prolonged droughts on water resources, agriculture, and vulnerable communities. Accurate climate data is vital for effective policymaking in arid areas facing climate challenges. Notably, under different scenarios and future timeframes, the high-emission scenario consistently shows longer-lasting and less frequent drought events. For the period 2061–2100, both indices predict severe and prolonged drought events under both emission scenarios, extending even to less vulnerable areas like the western coastal region by the end of the 21st century. This aligns with prior research (Zhai et al., 2020; Li et al., 2021), which indicates a global shift towards drier conditions with more severe and extended droughts when emissions increase under shared socioeconomic pathways (SSP1–2.6 and SSP5–8.5). Our findings affirm the heightened risk of future drought in arid and semi-arid regions. Due to intensified emission pathways, rising temperatures, and decreased precipitation, drought intensification zones in Syria may expand. Some previously humid areas in the west could transition into semi-humid or semi-dry regions, experiencing more severe and prolonged droughts (Homsi et al., 2021). Similar results were observed by Cook et al. (2020), who identified an increasing risk of drought severity in subtropical and mid-latitude regions due to reduced precipitation, increased temperatures, and higher evapotranspiration (Dai, 2013). The growing risk of droughts in Syria, exacerbated by future climate changes, underscores the need for mitigation strategies and reliable risk assessments on national and regional scales. These output results serve as a foundational basis for evidence-based strategies, identifying vulnerable areas, guiding agricultural adaptation planning, enhancing water resource management, and ensuring food security against drought impacts in Syria. High uncertainty in dry season precipitation projections, especially in semi-arid regions, is a complex challenge. Ukkola et al. (2020) emphasised the intricacies tied to these projections, involving factors like shifting weather patterns and nearby oceanic influences. This uncertainty complicates planning for water resources, agriculture, and more, urging the necessity of enhanced research and modeling for more accurate projections in semi-arid areas to address climate change impacts. Comprehending future drought patterns is critical for effective water resource management and improving the accuracy of

Syria's existing drought early warning system. Promoting climate education and increasing awareness among local communities about climate change and disaster risk is recommended to bolster resilience and enhance adaptive capacity to climate change throughout the region.

CRediT authorship contribution statement

Lopez Bustins Joan Albert: Supervision, Writing – review & editing. **Martin-Vide Javier:** Funding acquisition, Project administration, Supervision, Writing – review & editing. **Mathbout Shifa:** Conceptualization, Data curation, Formal analysis, Investigation, Methodology, Software, Visualization, Writing – original draft.

Declaration of Competing Interest

The authors declare the following financial interests/personal relationships which may be considered as potential competing interests: Shifa Mathbout reports financial support was provided by University of Barcelona. Shifa Mathbout reports a relationship with University of Barcelona that includes: board membership and funding grants.

Data Availability

The data that has been used is confidential.

Acknowledgments

This study was achieved within the framework of the EXE Project (PID2020-116860RB-C21/AEI/10.13039/501100011033) Spanish Ministry of Science and Innovation and the Climate Change and Landscape Ecology Group (former Climatology Group) of the University of Barcelona (2021 SGR 00310, Catalan Government).

Appendix A. Supporting information

Supplementary data associated with this article can be found in the online version at doi:10.1016/j.ejrh.2023.101581.

References

Aadhar, S., Mishra, V., 2017. High-resolution near real-time drought monitoring in South Asia. Sci. Data 4, 170145. https://doi.org/10.1038/sdata.2017.145.
Abel, G.J., Brottrager, M., Cuaresma, J.C., Muttarak, R., 2019. Climate, conflict and forced migration. Glob. Environ. Change 54, 239–249. https://doi.org/10.1016/j.gloenvcha.2018.12.003.
Abou Zakhem, A., Hafez, R., 2010. Climatic factors controlling chemical and isotopic characteristics of precipitation in Syria. Hydrol. Process. 24 (18), 2641–2654. https://doi.org/10.1002/hyp.7646.
Adeyeri, O.E., Zhou, W., Laux, P., Ndehedehe, C.E., Wang, X., Usman, M., Akinsanola, A.A., 2023. Multivariate drought monitoring, propagation, and projection using bias-corrected General Circulation Models. Earth's Future 11 (4), e2022EF003303. https://doi.org/10.1029/2022EF003303.
Adger, W.N., de Campos, R.S., Siddiqui, T., Gavonel, M.F., Szaboova, L., Rocky, M.H., Bhuiyan, M.R.A., Billah, T., 2021. Human security of urban migrant populations affected by length of residence and environmental hazards. J. Peace Res. 58 (1), 50–66. https://doi.org/10.1177/0022343320973717.
Almazroui, M., Saeed, S., Saeed, F., Islam, M.N., Ismail, M., 2020. Projections of precipitation and temperature over the South Asian Countries in CMIP6. J. Earth Syst. Sci. 4, 297–320. https://doi.org/10.1007/s41748-020-00157-7.
Almazroui, M., Ashfaq, M., Islam, M.N., Rashid, I.U., Kamil, S., Abid, M.A., O'Brien, E., Ismail, M., Simões Reboita, M., Sörensson, A.A., Arias, P.A., Muniz Alves, L., Tippett, M.K., Saeed, S., Haarsma, R., Doblas-Reyes, F.J., Saeed, F., Kucharski, F., Nadeem, I., Silva-Vidal, Y., Rivera, J.A., Azhar Ehsan, M., Martínez-Castro, D., Muñoz, A.G., Ali, A., Coppola, E., Bamba Sylla, M., 2021. Assessment of CMIP6 performance and projected temperature and precipitation changes over South America. J. Earth Syst. Sci. 5, 155–183. https://doi.org/10.1007/s41748-021-00233-6.
Alsafadi, Ansari, N., Mokhtar, A., Mohammed, S., Elbeltagi, A., Sammen, S.S., B i, S., 2022. An evapotranspiration deficit-based drought index to detect variability of terrestrial carbon productivity in the Middle East. Environ. Res. Lett. 17, 014051 https://doi.org/10.1088/1748-9326/ac4765.
Ayugi, B., Jiang, Z., Zhu, H., Ngoma, H., Babaousmail, H., Karim, R., Dike, V., 2021. Comparison of CMIP6 and CMIP5 models in simulating mean and extreme precipitation over East Africa. Int. J. Climatol. 41 6474–6496. https://doi.org/10.1002/joc.7207.
Ayugi, B., Jiang, Z., Iyakaremye, V., Ngoma, H., Babaousmail, H., Onyutha, C., Dike, V.N., Mumo, R., Ongoma, V., 2022. East African population exposure to precipitation extremes under 1.5 °C and 2.0 °C warming levels based on CMIP6 models. Environ. Res. Lett. 17, 044051 https://doi.org/10.1088/1748-9326/ac5d9d.
Ballarin, A.S., Barros, G.L., Cabrera, M.C., Wendland, E.C., 2021. A copula-based drought assessment framework considering global simulation models. J. Hydrol. Reg. Stud. 38, 100970 https://doi.org/10.1016/j.ejrh.2021.100970.
Barcikowska, M.J., Kapnick, S.B., Krishnamurty, L., Russo, S., Cherchi, A., Folland, C.K., 2020. Changes in the future summer Mediterranean climate: contribution of teleconnections and local factors. Earth Syst. Dyn. 11, 161–181. https://doi.org/10.5194/esd-13-321-2022.
Barlow, M., Zaitchik, B., Paz, S., Black, E., Evans, J., Hoell, A.A., 2016. Review of drought in the middle east and southwest Asia. J. Clim. 29, 8547–8574. https://doi.org/10.1175/JCLI-D-13-00692.1.
Beguería, S., Vicente-Serrano, S.M., Reig, F., Latorre, B., 2014. Standardized Precipitation Evapotranspiration Index (SPEI) Revisited: parameter fitting, evapotranspiration models, tools, datasets and drought monitoring. Int J. Clim. 34, 3001–3023. https://doi.org/10.1002/joc.3887.
Bi, D., Dix, M., Marsland, S., O'Farrell, S., Sullivan, A., Bodman, R., Law, R., Harman, I., Srbinovsky, J., Rashid, H., Dobrohotoff, P., Mackallah, C., Yan, H., Hirst, A., Savita, A., Dias, F.B., Woodhouse, M., Fiedler, R., Heerdegen, A., 2020. Configuration and spin-up of ACCESS-CM2, the new generation Australian Community Climate and Earth System Simulator Coupled Model. J. South. Hemisph. Earth Syst. Sci. 70 (1), 225–251. https://doi.org/10.1071/ES19040.
Breinl, K., Di Baldassarre, G., Mazzoleni, M., Lun, D., Vico, G., 2020. Extreme dry and wet spells face changes in their duration and timing. Environ. Res. Lett. 15, 074040 https://doi.org/10.1088/1748-9326/ab7d05.

Brogli, R., Sørland, S.L., Kröner, N., Schär, C., 2019. Causes of future Mediterranean precipitation decline depend on the season. Environ. Res. Lett. 14, 114017 https://doi.org/10.1088/1748-9326/ab4438.
Cammarano, D., Ceccarellib, S., Grando, S., Romagosa, I., Benbelkaceme, A., Akarf, T., Yassin, A., Pecchionihi, N., Franciai, E., Ronga, D., 2019. The impact of climate change on barley yield in the Mediterranean basin. Eur. J. Agron. 106 https://doi.org/10.1016/j.eja.2019.03.002.
Cannon, A.J., Sobie, S.R., Murdock, T.Q., 2015. Bias correction of GCM precipitation by quantile mapping: How well do methods preserve changes in quantiles and extremes? J. Clim. 28 (17), 6938–6959. https://doi.org/10.1175/JCLI-D-14-00754.1.
Cao, L., Xu, C., Suo, N., Song, L., Lei, X., 2023. Future dry-wet climatic characteristics and drought trends over arid Central Asia. Front. Earth Sci. 11, 1102633 https://doi.org/10.3389/feart.2023.1102633.
Cherchi, A., Fogli, P.G., Lovato, T., Peano, D., Iovino, D., Gualdi, S., Masina, S., Scoccimarro, E., Materia, S., Bellucci, A., Navarra, A., 2019. Global mean climate and main patterns of variability in the CMCC-CM2 Coupled Model. J. Adv. Model. Earth Syst. 11 (1), 185–209. https://doi.org/10.1029/2018MS001369.
Cook, B.I., Mankin, J.S., Marvel, K., Williams, A.P., Smerdon, J.E., Anchukaitis, K.J., 2020. Twenty-first century drought projections in the CMIP6 forcing scenarios. Earth'S. Future 8 (6), e2019EF001461. https://doi.org/10.1029/2019EF001461.
Cos, J., Doblas-Reyes, F., Jury, M., Marcos, R., Bretonnière, P.-A., Samsó, M., 2022. The Mediterranean climate change hotspot in the CMIP5 and CMIP6 projections. Earth Syst. Dyn. 13, 321–340. https://doi.org/10.5194/esd-13-321-2022.
Cramer, W., Guiot, J., Fader, M., Garrabou, J., Gattuso, J.P., Iglesias, A., Lange, M.A., Lionello, P., Llasat, M.C., Paz, S., Peñuelas, J., Snoussi, M., Toreti, A., Tsimplis, M.N., Xoplaki, E., 2018. Climate change and interconnected risks to sustainable development in the Mediterranean. Nat. Clim. Change 8, 972–980. https://doi.org/10.1038/s41558-018-0299-2.
Crocetti, L., Forkel, M., Fischer, M., Jurecka, F., Grlj, A., Salentinig, A., Trnka, M., Anderson, M., Ng, W.T., Kokalj, i, Bucur, A., Dorigo, W., 2020. Earth Observation for agricultural drought monitoring in the Pannonian Basin (southeastern Europe): current state and future directions. Reg. Environ. Change 20, 123. https://doi.org/10.1007/s10113-020-01710-w.
Dai, A., 2013. Increasing drought under global warming in observations and models. Nat. Clim. Change 3 (1), 52–58. https://doi.org/10.1038/nclimate1633.
Dai, M., Huang, S., Leng, G., Guo, Y., Wang, L., Fan, W., Li, P., Zheng, X., 2020. Assessing agricultural drought risk and its dynamic evolution characteristics. Agric. Water Manag. 231 (24), 106003 https://doi.org/10.1016/j.agwat.2020.106003.
Deng, K.Q., Azorin-Molina, C., Yang, S., Hu, C.D., Zhang, G.F., Minola, L., Vicente-Serrano, S., Chen, D., 2022. Shifting of summertime weather extremes in Western Europe during 2012–2020. Adv. Clim. Chang. Res. 13 (2), 218–227. https://doi.org/10.1016/j.accre.2022.01.008.
Dike, V.N., Lin, Z., Kece, F., Langendijk, G.S., Nath, D., 2022. Evaluation and multi-model projection of seasonal precipitation extremes over Central Asia based on CMIP6 simulations. Int J. Clim. 42 (14), 7228–7258. https://doi.org/10.1002/joc.7641.
Dosio, A., Lennard, C., Spinoni, J., 2022. Projections of indices of daily temperature and precipitation based on bias-adjusted CORDEX-Africa regional climate model simulations. Clim. Change 170, 13. https://doi.org/10.1007/s10584-022-03307-0.
Eyring, V., Bony, S., Meehl, G.A., Senior, C., Stevens, B., Stouffer, R.J., Taylor, K.E., 2016. Overview of the coupled model intercomparison project phase 6 (CMIP6) experimental design and organisation. Geosci. Model Dev. 8, 1937–1958. https://doi.org/10.5194/gmdd-8-10539-2015.
Fuentes, I., Padarian, J., Vervoort, R.W., 2022. Spatial and temporal global patterns of drought propagation. Front. Environ. Sci. 10 https://doi.org/10.3389/fenvs.2022.788248.
Fung, K.F., Huang, Y.F., Koo, C.H., 2020. Assessing drought conditions through temporal pattern, spatial characteristic and operational accuracy indicated by SPI and SPEI: case analysis for Peninsular Malaysia. Nat. Hazards 103, 2071–2101. https://doi.org/10.1007/s11069-020-04072-y.
Gudmundsson, L., Bremnes, J.B., Haugen, J.E., Engenskaugen, T., 2012. Technical note: downscaling RCM precipitation to the station scale using statistical transformations—A comparison of methods. Hydrol. Earth Syst. Sci. 16, 3383–3390. https://doi.org/10.5194/hess-16-3383-2012.
Hajima, T., Watanabe, M., Yamamoto, A., Tatebe, H., Noguchi, M.A., Abe, M., Ohgaito, R., Ito, A., Yamazaki, D., Okajima, H., Ito, A., Takata, K., Ogochi, K., Watanabe, S., Kawamiya, M., 2020. Development of the MIROC-ES2L Earth system model and the evaluation of biogeochemical processes and feedbacks. Geosci. Model Dev. 13, 2197–2244. https://doi.org/10.5194/gmd-13-2197-2020.
Hamed, K., 2008. Trend detection in hydrologic data: the mann-kendall trend test under the scaling hypothesis. J. Hydrol. 349, 350–363. https://doi.org/10.1016/j.jhydrol.2007.11.009.
Hargreaves, G.H., Samani, Z.A., 1985. Reference crop evapotranspiration from temperature. Appl. Eng. Agric. 1, 96–99.
Harris, I., Osborn, T.J., Jones, P., Lister, D., 2020. Version 4 of the CRU TS monthly high-resolution gridded multivariate climate dataset. Sci. Data. 7, 109 https://doi.org/10.1038/s41597-020-0453-3.
Homsi, R., Shahid, S., Iqbal, Z., Ali, A.M., Ali, G.F., 2021. Historical trends in crop water demand over semiarid region of Syria. Theor. Appl. Climatol. 146, 555–566. https://doi.org/10.1007/s00704-021-03751-5.
Houmsi, M.R., Shiru, M.S., Nashwan, M.S., Ahmed, K., Ziarh, G.F., Shahid, S., Chung, E.-S., Kim, S., 2019. Spatial shift of aridity and its impact on land use of Syria. Sustainability 11, 7047. https://doi.org/10.3390/su11247047.
John, A., Douville, H., Ribes, A., Yiou, P., 2022. Quantifying CMIP6 model uncertainties in extreme precipitation projections. Weather. Weather. Clim. Extrem. 36, 100435 https://doi.org/10.1016/j.wace.2022.100435.
Kwon, M., Kwon, H.H., Han, D., 2019. Spatio-temporal drought patterns of multiple drought indices based on precipitation and soil moisture: a case study in South Korea. Int J. Clim. 39 (12), 4669–4687. https://doi.org/10.1002/joc.609.
Law, R.M., Ziehn, T., Matear, R.J., Lenton, A., Chamberlain, M.A., Stevens, L.E., Wang, Y.-P., Srbinovsky, J., Bi, D., Yan, H., Vohralik, P.F., 2017. The carbon cycle in the Australian Community Climate and Earth System Simulator (ACCESS-ESM1) – Part 1: Model description and pre-industrial simulation. Geosci. Model Dev. 10, 2567–2590. https://doi.org/10.5194/gmd-10-2567-2017.
Li, J., Miao, C., Wei, W., Zhang, G., Hua, L., Chen, Y., Wang, X., 2021. Evaluation of CMIP6 global climate models for simulating land surface energy and water fluxes during 1979–2014. Adv. Model. Earth Syst. 13 (6), e2021MS002515 https://doi.org/10.1029/2021MS002515.
Lionello, P., Scarascia, L., 2018. The relation between climate change in the Mediterranean region and global warming. Reg. Environ. Change 18, 1481–1493. https://doi.org/10.1007/s10113-018-1290-1.
Lionello, P., Malanotte-Rizzoli, P., Boscolo, R. (Eds.), 2006. Mediterranean climate variability. Elsevier, Amsterdam.
Liu, Z., Wang, Y., Shao, M., Jia, X., Li, X., 2016. Spatiotemporal analysis of multiscalar drought characteristics across the Loess Plateau of China. J. Hydrol. 534, 281–299. https://doi.org/10.1016/j.jhydrol.2016.01.003.
Lurton, T., Balkanski, Y., Bastrikov, V., Bekki, S., Bopp, L., Braconnot, P., Brockmann, P., Cadule, P., Contoux, C., Cozic, A., Cugnet, D., Jean-Louis Dufresne, J.L., Éthé, C., Foujols, M.A., Ghattas, J., Hauglustaine, D., Hu, R.M., Kageyama, M., Khodri, M., Lebas, N., Levavasseur, G., Marchand, M., Ottlé, C., Peylin, P., Sima, A., Szopa, S., Thiéblemont, R., Vuichard, N., Boucher, O., 2020. Implementation of the CMIP6 forcing data in the IPSL-CM6A-LR model. J. Adv. Model. 12 https://doi.org/10.1029/2019MS001940.
Maraun, D., 2013. Bias correction, quantile mapping, and downscaling: revisiting the inflation issue. J. Clim. 26, 2137–2143. https://doi.org/10.1175/JCLI-D-12-00821.1.
Martel, J.L., Brissette, F.B., Picher, P.L., Troin, M., 2021. Climate Change and Rainfall Intensity–Duration–Frequency Curves: Overview of Science and Guidelines for Adaptation, 03121001-12 J. Hydrol. Eng.. https://doi.org/10.1061/(ASCE)HE.1943-5584.0002122.
Mathbout, S., Lopez- Bustins, J.A., Martin-Vide, J., Bech, J., Rodrigoc, F.S., 2018. Spatial and temporal analysis of drought variability at several time scales in Syria during 1961–2012. Atmos. Res. 200 (1), 153–168. https://doi.org/10.1016/j.atmosres.2017.09.016.
Mathbout, S., Lopez-Bustins, J.A., Royé, D., Martin-Vide, J., 2021. Mediterranean-Scale Drought: Regional Datasets for Exceptional Meteorological Drought Events during 1975–2019. Atmosphere 12 (8), 941. https://doi.org/10.3390/atmos12080941.
McBride, L.A., Hope, A.P., Canty, T.P., Bennett, B.F., Tribett, W.R., Salawitch, R.J., 2021. Comparison of CMIP6 historical climate simulations and future projected warming to an empirical model of global climate. Earth Syst. Dyn. 12, 545–579. https://doi.org/10.5194/esd-12-545-2021.
McCabe, G.J., Palecki, M.A., Betancourt, J.L., 2004. Pacific and Atlantic Ocean influences on multidecadal drought frequency in the United States. Proc. Natl. Acad. Sci. USA 101, 4136–4141. https://doi.org/10.1073/pnas.0306738101.

McKee, T.B., Doesken, N.J., Kleist, J., 1993. The relationship of drought frequency and duration to time scales. Proceeding of the 8th Conference on Applied Climatology. American Meteorological Society, Boston, pp. 179–184.
McKee, T.B., Doesken, N.J., Kleist, J., 1995. Drought monitoring with Multiple Time scales. Proceeding of the Ninth Conference on Applied Climatology. American Meteorological Society, Dallas, TX, pp. 233–236.
Meinshausen, M., Vogel, E., Nauels, A., Lorbacher, K., Meinshausen, N., Etheridge, D.M., Fraser, P.J., Montzka, S.A., Rayner, P.J., Trudinger, C.M., Krummel, P.B., Beyerle, U., Canadell, J.G., Daniel, J.S., Enting, I.G., Law, R.M., Lunder, C.R., Reimann, S., Rubino, M., Velders, G.J.M., Vollmer, M.K., Wang, R.H.J., Weiss, R., 2017. Historical greenhouse gas concentrations for climate modelling (CMIP6). Geosci. Model Dev. 10 (5), 2057–2116. https://doi.org/10.5194/gmd-10-2057-2017.
Meng, Y., Hao, Z., Feng, S., Guo, Q., Zhang, Y., 2022. Multivariate bias corrections of CMIP6 model simulations of compound dry and hot events across China. Earth Syst. Dyn. 17, 104005 https://doi.org/10.1088/1748-9326/ac8e86.
Merabti, A., Darouich, H., Paredes, Meddi, M., Pereira, S., 2023. Assessing spatial 596 variability and trends of droughts in Eastern Algeria Using SPI, RDI, PDSI, and MedPDSI-A597 novel drought index using the FAO56 evapotranspiration method. Water 15 (4), 626. https://doi.org/10.3390/w15040626, 598.
Miao, C., Duan, Q., Sun, Q., Huang, Y., Kong, D., Yang, T., Ye, A., Di, Z., Gong, W., 2014. Assessment of CMIP5 climate models and projected temperature changes over Northern Eurasia. . Environ. Res. Lett. 9 https://doi.org/10.1088/1748-9326/9/5/055007.
Mondal, S.K., Huang, J., Wang, Y., Su, B., Zhai, J., Tao, H., Wang, G., Fischer, T., Wen, S. Jiang, T., 2021. Doubling of the population exposed to drought over South Asia: CMIP6 multi-model-based analysis. Sci. Total Environ. 771, 145186. https://doi.org/10.1016/j.scitotenv.2021.145186.
My, L., Di Bacco, M., 2022. On the use of gridded data products for trend assessment and aridity classification in a mediterranean context: the case of the Apulia Region. Water 14. https://doi.org/10.3390/w14142203.
Ngoma, H., Wen, W., Ayugi, B., Babaousmail, H., Karim, R., Ongoma, V., 2021. Evaluation of rainfall simulations in CMIP6 models over Uganda. Int J. Climatol. 41, 4743–4768. https://doi.org/10.1002/joc.7098.
O'Neill, B.C., Kriegler, E., Ebi, K.L., Kemp-Benedict, E., Riahi, K., Rothman, D.S., van Ruijven, B.J., van Vuuren, D.P., Birkmann, J., Kok, K., Levy, M., Solecki,W, 2017. The roads ahead: narratives for shared socioeconomic pathways describing world futures in the 21st century. Glob. Environ. Change 42, 169–180. https://doi.org/10.1016/j.gloenvcha.2015.01.004.
Ozturk, T., Turp, M.T., Türkeş, M., Kurnaz, M.L., 2018. Future projections of temperature and precipitation climatology for CORDEX-MENA domain using RegCM4.4. Atmos. Res. 206 (107), 87. https://doi.org/10.1016/j.atmosres.2018.02.009.
Padrón, R.S., Gudmundsson, L., Decharme, B., Ducharne, A., Lawrence, D.A., Mao, J., Peano, D., Krinner, G., Kim, H., Seneviratne, S.I., 2020. Observed changes in dry-season water availability attributed to human-induced climate change. Nat. Geosci. 13, 477–481. https://doi.org/10.1038/s41561-020-0594-1.
Papalexiou, S.M., Montanari, A., 2019. Global and regional increase of precipitation extremes under global warming. Water Resour. Res. 55 (6), 4901–4914. https://doi.org/10.1029/2018WR024067.
Papalexiou, S.M., Rajulapati, C.R., Andreadis, K.M., Georgiou, E.F., Clark, M.P., Trenberth, K.E., 2021. Probabilistic evaluation of drought in CMIP6 simulations. Earth's Future 9. https://doi.org/10.1029/2021EF002150.
Papastefanou, P., Zang, C.S., Pugh, T.A.M., Liu, D., Grams, T.E.E., Hickler, T., Rammig, A., 2020. A dynamic model for strategies and dynamics of plant water-potential regulation under drought conditions. Front. Plant Sci. 11, 373. https://doi.org/10.3389/fpls.2020.00373.
Parsons, D.J., Reyb, D., Tanguy, M., Holman, I.P., 2019. Regional variations in the link between drought indices and reported agricultural impacts of drought. Agric. Syst. 173, 119–129. https://doi.org/10.1016/j.agsy.2019.02.015.
, 2020R Core Team., 2020. R: A language and environment for statistical computing. R Foundation for Statistical Computing. Vienna, Austria. https://www.R-project.org/.
Rajulapati, C.R., Papalexiou, S.M., 2023. Precipitation bias correction: a novel semi-parametric quantile mapping method. Earth Space Sci. 10 (4) https://doi.org/10.1029/2023EA002823.
Samani, Z.A., 2000. Estimating solar radiation and evapotranspiration using minimum climatological data. J. Irrig. Drain. 126 (4), 265–267. https://doi.org/10.1061/(ASCE)0733-9437(2000)126:4(265).
Séférian, R., Nabat, P., Michou, M., Saint-Martin, D., Voldoire, A., Colin, J., Decharme, B., Delire, C., Berthet, S., Chevallier, M., Sénési, S., Sarah, B., Matthieu, C., Laurent, F., Jessica, V., Marc, M., Emilie, J., Olivier, G., Jean- Francois, G., Pierre, M.M., Rym, M., Aurelien, R., Matthias, R., Romain, R., Melia David, S.Y., Emilia, S., Laurent, T., Sophie, V., Robin, W., Olivier, A., Laurent, B., Julie, D., Christian, E., Gurvan, M., 2019. Evaluation of CNRM earth system model, CNRM-ESM2-1: role of earth system processes in present-day and future climate. J. Adv. Model. Earth Syst. 12 (11), 4182–4227. https://doi.org/10.1029/2019MS001791.
Sharma, T., Vittal, H., Chhabra, S., Salvi, K., Ghosh, S., Karmakar, S., 2018. Understanding the cascade of GCM and downscaling uncertainties in hydro-climatic projections over India. Int. J. Climatol. 38, e178–e190. https://doi.org/10.1002/joc.5361.
Sheffield, J., Wood, E.F., 2011. Drought: Past Problems and Future Scenarios. Earth scan Ltd., 1616 P St. NW Washington DC. 20036, USA. ISBN 978–1-84971–082-4. 210 pp.
Singh, S., Ghosh, S., Sahana, A.S., Vittal, H., Karmakar, S., 2017. Do dynamic regional models add value to the global model projections of Indian monsoon? Clim. Dyn. 48, 1375–1397. https://doi.org/10.1007/s00382-016-3147-y.
Swart, N.C., Cole, J.N.S., Kharin, V.V., Lazare, M., Scinocca, J.F., Gillett, N.P., Anstey, J., Arora, V., Christian, J.R., Hanna, S., Jiao, Y., Lee, W.G., Majaess, F., Saenko, O.A., Seiler, C., Seinen, C., Shao, A., Sigmond, M., Solheim, L., Salzen, K.V., Yang, D., Winter, B., 2019. The Canadian Earth system model version 5 (CanESM5.0.3). Geosci. Model Dev. 12, 4823–4873. https://doi.org/10.5194/gmd-12-4823-2019.
Tebaldi, C., Ranasinghe, R., Vousdoukas, M., Rasmussen, D.J., Vega-Westhoff, B., Kirezci, E., Kopp, R.E., Sriver, R., Mentaschi, 2021. Extreme sea levels at different global warming levels. Nat. Clim. Change 11, 746–751. https://doi.org/10.1038/s41558-021-01127-1.
Thorarinsdottir, T.L., Sillmann, J., Haugen, M., Gissibl, N., Sandstad, M., 2020. Evaluation of CMIP5 and CMIP6 simulations of historical surface air temperature extremes using proper evaluation methods. Environ. Res. Lett. 15, 124041 https://doi.org/10.1088/1748-9326/abc778.
Tong, Y., Gao, X., Han, Z., Xu, Y., Xu, Y., Giorgi, F., 2021. Bias correction of temperature and precipitation over China for RCM simulations using the QM and QDM methods. Clim. Dyn. 57 (5–6), 1425–1443. https://doi.org/10.1007/s00382-020-05447-4.
Tramblay, Y., Koutroulis, A., Samaniego, L., Vicente-Serrano, S.M., Volaire, F., Boone, A., Page, M.L., Llasat, M.C., Albergel, C., Burak, S., Cailleret, M., Kalin, K.C., Davi, H., Dupuy, J.L., Greve, P., Grillakis, M., Jarlan, L., Martin-StPaul, N., Vilalta, J.M., Mouillot, F., Velazquez, D.P., Quintana-Seguí, P., Renard, D., Turco, M., Türkes, M., 2020. Challenges for drought assessment in the Mediterranean region under future climate scenarios. Environ. Earth Sci. 210, 103348 https://doi.org/10.1016/j.earscirev.2020.103348.
Tsakiris, G., Kordalis, N., Tigkas, D., Tsakiris, V., Vangelis, H., 2016. Analysing drought severity and areal extent by 2D Archimedean copulas. Water Resour. Res. 30, 1–13. https://doi.org/10.1007/s11269-016-1543-z.
Tuel, A., Eltahir, E.A.B., 2020. Why is the Mediterranean a climate change hot spot? J. Clim. 33 (14), 5829–5843. https://doi.org/10.1175/JCLI-D-19-0910.1.
Ukkola, A.M., Pitman, A.J., De Kauwe, M.G., Abramowitz, G., Herger, N., Evans, J.P., Decker, M., 2018. Evaluating CMIP5 model agreement for multiple drought metrics. J. Hydrometeorol. 19, 969–988.
Ukkola, A.M., De Kauwe, M.G., Roderick, M.L., Abramowitz, G., Pitman, A.J., 2020. Robust future changes in meteorological drought in CMIP6 projections despite uncertainty in precipitation. Geophys. Res. Lett. 10 https://doi.org/10.1029/2020GL087820.
Valipour, M., Gholami Sefidkouhi, M., Raeini-Sarjaz, M., 2020. Spatiotemporal analysis of reference evapotranspiration in arid, semiarid, mediterranean and very humid climates considering developed models and lysimeter measurements. Water Sci. Eng. 5, 81–96. https://doi.org/10.1007/s41101-020-00087-5.
Van Vuuren, D., Edmonds, J., Kainuma, M., Riahi, K., Thomson, A., Hibbard, K., Hurtt, G., Kram, T., Krey, V., Lamarque, J.-F., Masui, T., Meinshausen, M., Nakicenovic, N., Smith, S., Rose, S., 2011. The representative concentration pathways: an overview. Clim. Change 109, 5–31. https://doi.org/10.1007/s10584-011-0148-z.

Vicente-Serrano, S.M., Begueria, S., Lopez-Moreno, J.I., Angulo, M., Kenawy, E.L., 2010. A new global 0.58 gridded dataset (1901–2006) of a multiscalar drought index: comparison with current drought index datasets based on the Palmer drought severity index. J. Hydrometeorol. 11, 1033–1043. https://doi.org/10.1175/2010JHM1224.1.

Voldoire, A., Saint-Martin, D., Sénési, S., Guérémy, F., Michou, M., Moine, M.P., Nabat, P., Roehrig, R., Salas y Mélia, D., Séférian, R., Valcke, S., Beau, I., Belamari, S., Berthet, S., Cassou, C., Cattiaux, J., Deshayes, J., Douville, H., Ethé, C., Franchistéguy, L., Geoffroy, O., Lévy, C., Madec, G., Meurdesoif, Y., Msadek, R., Ribes, A., Sanchez-Gomez, E., Terray, L., Waldman, R., 2019. Evaluation of CMIP6 DECK Experiments With CNRM-CM6-1. J, Adv. Model. Earth Syst. 11 (7), 2177–2213. https://doi.org/10.1029/2019MS001683.

Wild, M., 2020. The global energy balance as represented in CMIP6 climate models. Clim. Dyn. 55 (3), 553–577. https://doi.org/10.1007/s00382-020-05282-7.

Wu, J., Chen, X., Yao, H., Zhang, D., 2021. Multi-timescale assessment of propagation thresholds from meteorological to hydrological drought. Sci. Total Environ. 765, 144232 https://doi.org/10.1016/j.scitotenv.2020.144232.

Wu, T., Lu, Y., Fang, Y., Xin, X., Li, L., Li, W., Jie, W., Zhang, J., Liu, Y., Zhang, L., Zhang, F., Zhang, Y., Wu, F., Li, J., Chu, M., Wang, Z., Shi, X., Liu, X., Wei, M., Huang, A., Zhang, Y., Liu, X., 2019. The Beijing Climate Center Climate System Model (BCC-CSM): the main progress from CMIP5 to CMIP6. Geosci. Model Dev. 12, 1573–1600. https://doi.org/10.5194/gmd-12-1573-2019.

Xu, H.J., Wang, X.P., Zhao, Z.Y., 2021. Drought sensitivity of vegetation photosynthesis along the aridity gradient in northern China. Int. J. Appl. Earth Obs. Geoinf. 102, 102418. https://doi.org/10.1016/j.jag.2021.102418.

Xu, P., Zhang, C., Wen, Z., Park, E., Jakada, H., 2022. Climate variability impacts on runoff projection under quantile mapping bias correction in the support CMIP6: an investigation in Lushi basin of China. J. Hydrol. 614 (B), 128550 https://doi.org/10.1016/j.jhydrol.2022.128550.

Yang, T., Ding, J., Liu, D., Wang, X., Wang, T., 2019. Combined use of multiple drought indices for global assessment of dry gets drier and wet gets wetter paradigm. J. Clim. 32 (3), 737–748. https://doi.org/10.1175/JCLI-D-18-0261.1.

Yukimoto, S., Kawai, H., Koshiro, T., Oshima, N., Yoshida, K., Urakawa, S., Tsujino, H., Deushi, M., Tanaka, T., Hosaka, M., Yabu, S., Yoshimura, H., Shindo, E., Mizuta, R., Obata, A., Adachi, Y., Ishii, M., 2019. The meteorological research institute earth system model version 2.0, MRI-ESM2.0: Description and basic evaluation of the physical component. J. Meteorol. Soc. Jpn. 97 (5) https://doi.org/10.2151/jmsj.2019-051.

Zhai, J., Kumar, S., Fischer, T., Fischer, Y., Su, Buda, Huang, J., Tao, H., Wang, Su, B., Huang, J., Tao, H., Wang, G., Ullah, W., Jalal Uddine, M.D., 2020. Future drought characteristics through a multi-model ensemble from CMIP6 over South Asia. Atmos. Res. 246, 10511. https://doi.org/10.1016/j.atmosres.2020.105111.

Zhang, L., Jiao, W., Zhang, H., Huang, C., Tong, Q., 2017. Studying drought phenomena in the Continental United States in 2011 and 2012 using various drought indices. Remote Sens. Environ. 190, 96–106. https://doi.org/10.1016/j.rse.2016.12.010.

Zhao, T., Dai, A., 2022. CMIP6 model-projected hydroclimatic and drought changes and their causes in the twenty-first century. J. Clim. 35 (3), 897–921. https://doi.org/10.1175/JCLI-D-21-0442.1.

Zhong, L., Hua, L., Yan, Z., 2020. Datasets of meteorological drought events and risks for the developing countries in Eurasia. Earth Syst. Sci. Data 4, 191–223. https://doi.org/10.1080/20964471.2019.1710383.